ACS NANO

www.acsnano.org

REVIEW

Next-Generation Ultrafiltration Membranes Enabled by Block Polymers

Nicholas Hampu, Jay R. Werber, Wui Yarn Chan, Elizabeth C. Feinberg, and Marc A. Hillmyer*

Cite This: *ACS Nano* 2020, 14, 16446–16471

Read Online

ACCESS | Metrics & More | Article Recommendations | Supporting Information

ABSTRACT: Reliable and equitable access to safe drinking water is a major and growing challenge worldwide. Membrane separations represent one of the most promising strategies for the energy-efficient purification of potential water sources. In particular, porous membranes are used for the ultrafiltration (UF) of water to remove contaminants with nanometric sizes. However, despite exhibiting excellent water permeability and solution processability, existing UF membranes contain a broad distribution of pore sizes that limit their size selectivity. To maximize the potential utility of UF membranes and allow for precise separations, improvements in the size selectivity of these systems must be achieved. Block polymers represent a potentially transformative solution, as these materials self-assemble into well-defined domains of uniform size. Several different strategies have been reported for integrating block polymers into UF membranes, and each strategy has its own set of materials and processing considerations to ensure that uniform and continuous pores are generated. This Review aims to summarize and critically analyze the chemistries, processing techniques, and properties required for the most common methods for producing porous membranes from block polymers, with a particular focus on the fundamental mechanisms underlying block polymer self-assembly and pore formation. Critical structure–property–performance metrics will be analyzed for block polymer UF membranes to understand how these membranes compare to commercial UF membranes and to identify key research areas for continued improvements. This Review is intended to inform readers of the capabilities and current challenges of block polymer UF membranes, while stimulating critical thought on strategies to advance these technologies.

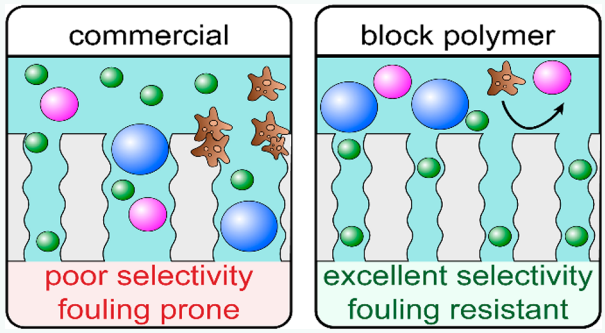

KEYWORDS: *block polymers, ultrafiltration, permeability–selectivity, isoporous, SNIPS, self-assembly, water filtration, membranes, antifouling*

INTRODUCTION

Reliable access to clean water is essential to both human health and global stability. However, approximately 4 billion people experience water scarcity for at least 1 month of the year.[1] Global water demand is expected to expand 20–30% by 2050 due to population growth and industrialization, while climate change is expected to further disrupt the supply of clean water.[1,2] Therefore, equitable access to clean water will benefit from the utilization of all available water sources, including the energy-efficient treatment of municipal and industrial wastewater. Selective membrane technologies will play a critical role in developing a sustainable water economy.[3−8]

Membrane technologies are typically classified according to their effective pore size and separation mechanism. Ultrafiltration (UF) membranes, with pore sizes in the 1−100 nm range, are of particular interest for drinking water and wastewater treatment.[3,7,9] These nanoscale pores are ideal for rejecting wastewater contaminants, such as viruses, microbes, colloidal particles, and natural organic matter, according to their hydrodynamic size.[9] Consequently, UF membranes have found utility in decontamination of drinking water, wastewater treatment, and membrane bioreactors, providing higher quality filtered water than traditional treatment processes.[7] Additionally, UF membranes are critical tools in certain industrial processes (*e.g.*, bioprocessing, dairy processing), enabling low-cost and highly efficient separations.

Most commercial UF membranes are fabricated from homopolymer solutions using non-solvent-induced phase separation (NIPS).[3,5,10] NIPS membranes exhibit continuous pores, thin selective layers, and high water permeability, but their broad pore size distribution can limit their size selectivity

Received: September 18, 2020
Accepted: November 24, 2020
Published: December 14, 2020

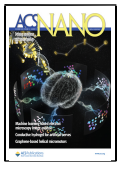

https://dx.doi.org/10.1021/acsnano.0c07883
ACS Nano 2020, 14, 16446–16471

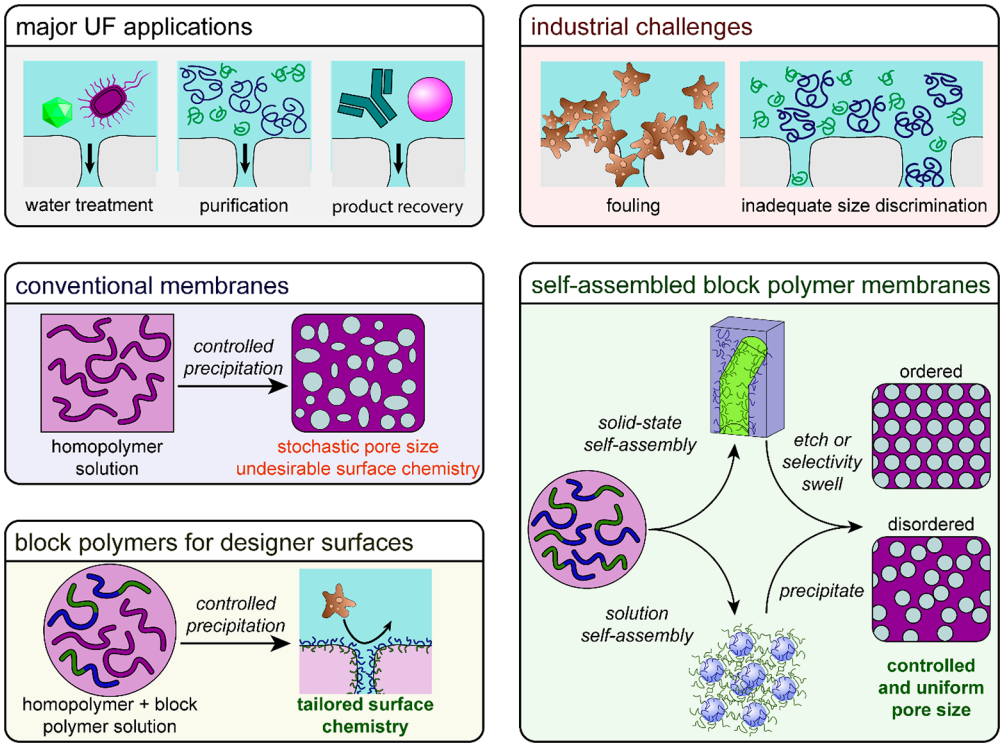

Figure 1. Ultrafiltration (UF) membranes find extensive commercial use in water purification, macromolecular separations, and product recovery in the process industry. However, next-generation applications for UF membranes are limited by the stochastic pore sizes and undesirable surface chemistries of current commercial membranes produced by non-solvent-induced phase separation (NIPS), resulting in inadequate separations and poor fouling resistance. Therefore, the tailored surface chemistries and uniform pore sizes enabled by block polymers offer the potential to expand the utility of UF membranes to applications that require precise separations and challenging feed solutions. Block polymers can be easily incorporated into existing NIPS formulations to tailor surface chemistry and mitigate fouling. Additionally, block polymers can be directly integrated as the active layer in UF membranes, where solid-state or solution self-assembly templates the generation of uniform pores with either an ordered or disordered arrangement.

and thus their utility for demanding and highly efficient separations.[3,5,11,12] Alternatively, track-etched membranes display nearly uniform pore sizes and improved size selectivity, but their low surface porosities and large thicknesses result in low water permeability. The ideal UF membrane would combine the high porosity and thin selective layers of NIPS membranes with the uniform pore sizes of track-etched membranes. Block polymers, comprising two or more chemically distinct polymers covalently linked into a single chain, potentially provide a path to such a system due to their self-assembly into regular and periodic nanostructures of nearly uniform size.[7,13−15] By tuning the composition of the block polymer, a number of ordered morphologies (*i.e.*, cylinders, gyroid, lamellae) with well-connected domains can be obtained and subsequently converted into continuous and uniform pores using various strategies.[6,7] Additionally, amphiphilic block polymers containing both hydrophobic and hydrophilic polymer blocks enhance the hydrophilicity and functionality of the membrane surface and pores as compared to homopolymer-derived NIPS membranes, increasing fouling resistance and operation lifetime.[16,17]

Solution processing techniques combined with amenable polymer chemistries are central to controlling the structure of block polymer membranes.[18−21] The primary objective is to ultimately produce pores of uniform size from the self-assembled block polymer domains. Achieving such a goal often requires careful design of the film casting process and, frequently, additional post-fabrication processes to produce homogeneous domains that span the entire thickness of the block polymer layer.[18,21−23] These processes must be carefully optimized to maximize the water permeability, size selectivity, and process scalability. Membrane properties are highly dependent upon the polymer chemistry, processing conditions, and pore formation mechanism. Further developments in scalable and cost-effective methods to produce high-performing membranes are essential for block polymers to achieve commercial success and positively impact water treatment processes.[18,23,24] Figure 1 presents an illustration of the key applications and features of block polymer UF membranes in comparison to commercial NIPS membranes.

In this Review, we critically examine the state of the art in block polymer membrane fabrication; assess membrane performance to date; and identify areas that, in our view, require further improvement to produce commercially viable membranes. We first introduce several key applications of UF membranes in terms of their desired properties and then discuss commonly employed strategies for block polymer UF membrane fabrication through the lens of materials needs, fundamental mechanistic principles, and processing requirements. Finally, we examine key structure-processing-performance relationships of these membranes in the context of their water permeability, size selectivity, and fouling resistance. Through such relationships, we analyze how the performance of block polymer UF membranes compares to existing commercial UF membranes and use these data to identify crucial aspects that merit further fundamental research and

https://dx.doi.org/10.1021/acsnano.0c07883
ACS Nano 2020, 14, 16446−16471

Table 1. Common UF Processes and Important Membrane Properties

UF process	typical materials	typical water permeability (L m^{-2} h^{-1} bar^{-1})	typical pore size	targeted contaminants	operation lifetime
wastewater[27,36,37] and drinking water treatment[36−38]	PAN, PSF, PVDF	>200	∼20 nm	viruses, bacteria, particulates, pathogens	>5 y
RO pretreatment[27,32,36]	PAN, PSF, PVDF	>200	∼20 nm	viruses, bacteria, organic matter	>5 y
RO support layer[3,36,39]	PSF, PES	200−400	20 nm	ions, salts	up to 7 y
membrane bioreactors[40−43]	PE, PVDF, PTFE	>500	30 nm to 1 μm	bacteria, organic matter	8−10 y
virus filtration in bioprocessing[44,45]	PES, PVDF	∼500	15 nm	viruses	single use

practical development. This work is intended to provide a critical overview of the existing block polymer membrane literature, while also stimulating thought on how to push these technologies toward real-world application.

MEMBRANE PROPERTIES AND IMPORTANT APPLICATIONS

Principal Membrane Characteristics. For optimal performance in industrial applications, UF membranes must have sufficient water permeability, fouling resistance, size selectivity, and mechanical robustness. The pure water permeability, A, for UF membranes is the volumetric flux (volume flow per time per membrane area) of pure water normalized to the applied hydraulic pressure (pressure applied to the fluid, water in this case) and is given typically in liters per meter squared per hour per bar (L m^{-2} h^{-1} bar^{-1}). In the simplest model, the membrane is treated as a parallel array of tortuous capillaries using the Hagen−Poiseuille equation:[25]

$$A = \frac{\varepsilon r_p^2}{8\tau^2 \mu \delta_m} \quad (1)$$

Here, ε is the surface porosity, r_p is the pore radius, τ is the pore tortuosity, μ is the viscosity of water, and δ_m is the membrane (active layer) thickness. Equation 1 often shows A with a τ^{-1} dependence, only accounting for an increase in the effective path length for water permeation.[18,24,26] However, tortuosity increases both the effective path length of the capillaries and the capillary velocity and therefore results in a τ^{-2} dependence (see the Supporting Information for a derivation and discussion).[25]

Optimal membrane designs for permeability have thin active layers with high porosity and a macroporous substructure for mechanical support. High water permeabilities can allow for greater water fluxes or decreased applied pressure driving forces, thereby decreasing energy and equipment costs.[27] However, for many practical processes, hydraulic resistance from unstirred boundary layers in the feed channel (also called concentration polarization) and from fouling (buildup of organic matter on the surface of the membrane) can be substantial. Additionally, fouling is typically exacerbated by increased water flux.[28]

Fouling resistance and fouling mitigation are, therefore, critical considerations in membrane design.[3,29] Extensive fouling from the adhesion of biological, organic, and inorganic matter can result in pore blockage, decreased water permeability, and changes in the molecular weight cutoff (MWCO), which is conventionally defined as the lowest solute molecular weight (molar mass) where 90% solute rejection is observed.[27] The ideal UF membrane has a surface chemistry and topography engineered to prevent such adsorption, minimizing irreversible changes in the water permeability over the operation lifetime.[30,31] The charge of the membrane can also critically affect fouling resistance. For example, positively charged membranes are used to recover cationic latex paint in cathodic electrocoating processes, while negatively charged membranes lead to rapid fouling from the same particles.[32] Finally, many UF membranes are designed to allow for periodic backflushes or air scrubbing to sweep away foulant layers.[27,32] Hollow fiber geometries (capillaries with outer diameters of roughly 0.5−1 mm) are particularly advantageous in this regard. Facile backflushing and a high surface area/packing volume ratio make hollow fibers the main form factor used industrially.[27]

UF membranes mainly separate based on a molecular-sieve mechanism, where large solutes are excluded from entering the pore.[27] The primary selectivity metric is the MWCO. The selectivity of UF membranes is dictated by both the average pore size and the pore size distribution of the active layer, where the average pore size generally sets the MWCO and the pore size distribution governs the ability to discriminate between particles of similar size.[11,12] From a membrane selectivity perspective, an ideal membrane would be isoporous, having uniformly sized pores for precise separations. Selectivity for charged solutes is also affected by the charge (if any) of the membrane.[11] Tailored selectivities can be engineered by pore wall functionalization, for example, to facilitate affinity-driven separations.[33−35]

Finally, all of these considerations must be readily integrated into cost-effective manufacturing processes at industrially relevant size scales to realize their full potential. This requires systems that are compatible with roll-to-roll coating processes and the existing membrane fabrication infrastructure. Ideally, these technologies would also be compatible with fiber spinning processes to produce the hollow fiber form factor favored by industry. The relative importance of each of the above criteria is often highly dependent on the process in which they are employed. Several important applications of UF membranes are briefly examined in the following sections and are summarized in Table 1.

Water Treatment. Ultrafiltration plays a critical role in modern water treatment processes for drinking water, municipal wastewater, and pre-treatment for reverse osmosis.[36,46,47] In all of these processes, UF is used to remove suspended solids from water, yielding purified water as the desired product. Compared to conventional physical treatment steps (*e.g.*, granular filtration), UF allows for smaller-footprint facilities and higher water quality (*e.g.*, pathogen removal) across varying feedwater composition.[27,47] As mentioned above, hollow fiber membranes are the dominant form factor, and the UF process is either operated in cross-flow mode, where the retentate is recycled, or in dead-end filtration mode,

https://dx.doi.org/10.1021/acsnano.0c07883
ACS Nano 2020, 14, 16446−16471

where the retentate accumulates on the membrane surface. In both modes, backflushing is periodically used to remove sediment build-up on the membrane surface. In these processes, water flux is frequently 50−100 L m^{-2} h^{-1}, although increased fluxes up to 200 L m^{-2} h^{-1} are possible when the feedwater is relatively non-fouling.[36,37] Organic matter (*e.g.*, humic acid and carbohydrates) tends to be the main foulant.[48] UF membrane lifetimes in these plants are typically >5 years.[36]

Arguably the largest commercial application for UF membranes is in membrane bioreactors (MBRs) used to treat wastewater, with a current global treatment capacity estimated at 20 million m^3 d^{-1}.[49] MBRs combine biodegradation and ultrafiltration in a single process, resulting in several advantages over either process in isolation. MBRs can operate at significantly higher biomass concentrations than traditional activated sludge bioreactors,[50] resulting in more efficient biodegradation of organics with a smaller reactor footprint. The addition of a UF membrane also results in an effluent that is effectively free of biological contaminants, without the need for gravitational settling.[51] High size-selectivity is not the most critical aspect for applications in high-performing MBRs;[45] however, block polymers may still be beneficial for this application. The dominant failure mode of MBRs is irreversible fouling.[43] The incorporation of amphiphilic block polymers into MBRs presents an opportunity to minimize irreversible fouling in next-generation membranes, improving reactor lifetime and lowering operation costs.

In municipal drinking water treatment processes, surface waters (such as lakes, reservoirs, and rivers) or groundwater are treated using a series of physicochemical treatment steps (*e.g.*, flocculation, sedimentation, and granular filtration) designed to remove bacteria, viruses, and other suspended particles from solution.[27] Owing to its superior ability to remove pathogens, UF is widely being adopted in modern industrial drinking water treatment facilities, either fully supplanting the physical separation steps or serving as a final polishing step.[47] As of 2009, UF and larger pore-size microfiltration (MF) processes had a total capacity of ∼3 million m^3 d^{-1} in the United States, roughly equivalent to the household water use of ∼8 million people.[38]

Reverse osmosis (RO) is currently the most widespread and energy-efficient desalination technology and is also a central step in the potable reuse of municipal wastewater.[3,36] UF membranes provide mechanical support to the thin, cross-linked polyamide layers used in RO. The polyamide layer primarily dictates salt rejection and water permeability, but the effect of the UF support remains a subject of active research.[39] RO membranes are highly susceptible to fouling because of their surface chemistry and morphology. Furthermore, they are not easily backwashed and are typically not very stable to chemical cleaning, particularly with oxidizing chemicals such as chlorine. Therefore, UF is commonly used as pre-treatment to mitigate fouling of the RO membranes and to extend their lifetime.[36]

For each of the above water-treatment applications, key UF membrane characteristics include fouling resistance, the ability to be effectively cleaned, high water permeability, and relatively small pore sizes (*i.e.*, <20 nm in diameter) to allow for high rejection of viruses.[44] The chemically tailored anti-fouling surfaces possible for block polymer membranes could be advantageous for the highly fouling feed streams that are typical of water treatment. Variability in the membrane pore size is not ruinous for the overall UF performance, but it still has important ramifications on the permeability and selectivity. For example, a broader pore size distribution for a given water permeability will typically result in decreased retention of pathogens. Water permeabilities >200 L m^{-2} h^{-2} bar^{-1} are required to allow for high water fluxes at low pressures (<1 bar) and thus energy-efficient separations. The uniform pore sizes of block polymer membranes should facilitate more effective water treatment, provided that the water permeability is competitive with commercial NIPS membranes. However, UF is typically one of several purification processes used in water treatment facilities, with subsequent disinfection steps serving to inactivate residual pathogens that pass through the membrane. Consequently, the low size selectivity of existing NIPS membranes is generally not catastrophic, and the cost of block polymer membranes will likely need to approach the cost of conventional NIPS membranes to be competitive for water treatment. A summary of desirable attributes for UF membranes used in wastewater and drinking water filtration and in RO pre-treatment is provided in Table 1.

Process Industry. UF is extensively used in process industries for both industrial wastewater treatment and the separation of target solutes from impurity solutes.[27,32] Consequently, monodisperse pore sizes may be highly advantageous, allowing for more selective processes with better yield of the desired product and removal of impurities. UF membranes find major applications in the food and beverage (*e.g.*, dairy), metals and coatings, and bioprocessing industries.[27,32] For many of these processes, membranes with tailored chemistries and geometries for the target application are used. Specially designed membranes will be essential to enable new and emerging industrial applications.

The bioprocessing industry is a salient example of the need for specially designed membranes.[45] UF has two main applications in the production of protein therapeutics (*e.g.*, monoclonal antibodies). The first is virus filtration to remove viruses that may be present in the protein solution.[44] Highly selective membranes are needed, allowing the target protein (*e.g.*, monoclonal antibodies with diameters of ∼10 nm) to permeate while reducing the putative virus concentration >10,000-fold. Viruses vary in size according to class, ranging from ∼20 nm for parvoviruses to 300 nm for smallpox. Therefore, pores would ideally be entirely between 10 and 20 nm in diameter to ensure complete removal of all viruses and permeation of the target protein. To enable straightforward processing, virus filtration is operated in dead-end filtration mode. The second UF process is the final purification step, where the protein is concentrated and buffer exchanged into the final formulation buffer.[45] In this process, crossflow filtration with recirculation is performed using flat-sheet cassettes containing highly hydrophilic, fouling-resistant regenerated cellulose membranes with relatively small pore sizes to allow for high product retention. Water permeability is less important, as resistance from the protein gel layer dominates performance. A third potential application of UF is to replace the expensive affinity chromatography step, which uses protein-based ligands to reversibly bind the target antibody to separate it from other cellular impurities.[45] A process based on UF would separate based on size, retaining the relatively large antibody and letting smaller impurities flow through the membrane. The monodisperse pore sizes of block polymer membranes could dramatically improve the performance of a UF-based process. Therefore, process industries will

https://dx.doi.org/10.1021/acsnano.0c07883
ACS Nano 2020, 14, 16446−16471

likely include the first commercial applications of block polymer membranes with monodisperse pore sizes, as the costly and high-value products associated with these applications may merit the increased materials expenses of block polymers.

CURRENT STATE AND LIMITATIONS OF ULTRAFILTRATION MEMBRANES

Homopolymer Non-Solvent-Induced Phase Separation. To better understand the potential application of block polymers in UF membrane processes, it is necessary to review the processing and properties of existing commercial homopolymer membranes. The current standard for commercial polymeric UF membrane fabrication is non-solvent-induced phase separation (NIPS).[5] In the NIPS process, a concentrated homopolymer solution is cast into a film. This solvent-swollen film is then immersed into a non-solvent (typically water). The influx of non-solvent causes the polymer and solvent to de-mix, and the system phase separates into polymer-rich and polymer-poor domains, which ultimately become the membrane matrix and pores, respectively.[5,10]

Ultrafiltration membranes produced using NIPS exhibit an integral and asymmetric structure, where a thin active layer with small pores that separate contaminants gradually transitions into a thicker substructure with large pores that provide a high water permeability and sufficient mechanical integrity.[3,5] The ubiquity of NIPS membranes is a function of the simple solution casting processes used in their fabrication, enabling the cost-effective and large-scale production of membranes with high water permeabilities. The NIPS process is highly versatile and is amenable to a variety of polymer structures, such as polysulfone (PSF), polyethersulfone (PES), polyacrylonitrile (PAN), and poly(vinylidene fluoride) (PVDF), allowing the membrane properties to be tailored to the requirements of the targeted application.[5] Furthermore, the pore morphology and size can be rationally tuned through judicious selection of the polymer chemistry and concentration and through choice of solvent(s) and non-solvent(s) (Figure 2).[5,52]

The integrally structured and asymmetric architecture of NIPS membranes is highly desirable. Because the entire membrane is composed of a single material, the small surface pores that enable solute rejection are inherently connected to the larger pores in the substructure. This results in high water permeability, minimizing the membrane areal footprint and energy consumption and maximizing water filtration. However, the broad pore size distribution of NIPS membranes limits their growth potential.[3,4] Low size selectivity is undesirable for many high-value applications that require near-perfect discrimination between solutes of similar sizes. Furthermore, these membranes are generally made from hydrophobic polymers which are susceptible to surface fouling.[53] The addition of hydrophilic homopolymers, such as poly(vinylpyrrolidone), into the NIPS casting solution can improve membrane hydrophilicity and increase fouling resistance.[5] However, homopolymer additives are bound to the membrane matrix through weak physical interactions and can leach out over time, resulting in performance deterioration. To expand the practical applications of UF membranes and facilitate next generation technologies, significant improvements to the size selectivity and fouling resistance of UF membranes must be made without compromising their typically high water permeabilities and process scalability.

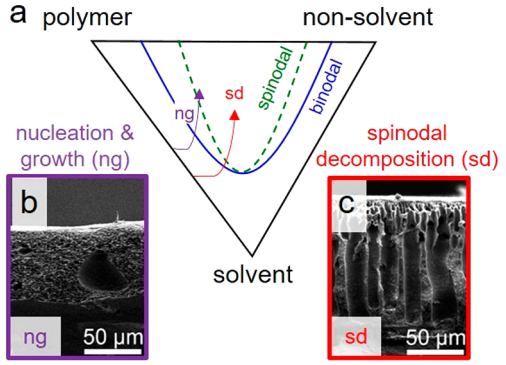

Figure 2. Sketch of a hypothetical ternary phase diagram illustrating two different precipitation paths for homopolymer NIPS solutions (a). The purple curve denotes a solution with a higher polymer concentration that forms a spongy microstructure. Upon crossing the binodal curve, polymer-rich and polymer-poor domains form by nucleation and growth, and these domains can vitrify before spinodal decomposition can proceed. A representative cross-sectional SEM image of such a system is presented in (b). The red curve in (a) denotes a solution with a lower polymer concentration that undergoes instantaneous de-mixing as it crosses the spinodal curve, resulting in a finger-like microstructure. A representative cross-sectional SEM image for such a system is presented in (c). Adapted with permission from ref 52. Copyright 2011 Elsevier.

Homopolymer NIPS with Surface Segregating Block Polymer Additives. To address limitations related to the surface chemistry of NIPS membranes, a variety of methods have been developed to coat or covalently graft hydrophilic polymers onto their surfaces. However, these approaches require additional processing steps, lack long-term stability, and can constrict pores.[54] High density and stable functionalization of both the internal pores and external surface can be achieved without compromising the water permeability by adding amphiphilic block and comb polymers into the NIPS casting solution. At early time points during NIPS, homopolymer at the casting solution/coagulation bath interface migrates to form a dense surface layer. Transport of the hydrophilic component in amphiphilic additives is slower due to its lower chemical potential, allowing it to be enriched at the solvent/non-solvent interface.[55] Surface segregation of the hydrophilic component at the membrane surface and pore walls has been confirmed by X-ray photoelectron spectroscopy (XPS).[55] Surface segregation prevents irreversible adsorption of hydrophobic contaminants onto the membrane, while the hydrophobic component anchors the block polymer to the membrane and helps mitigate leaching (Figure 3a). The microstructure of these membranes can be tuned by varying the amphiphile concentration (typically 2−20 wt%). Blends that contain a small amount of block polymer additive form dense skin layers with cellular substructures.[30,54] Both the porosity and density of macrovoids increase with additive concentration due to compatibilization of the casting solution with the non-solvent, which facilitates instantaneous de-mixing.[56]

The surface segregation method can be applied to a wide range of polymer chemistries used in NIPS membrane fabrication. The hydrophobic segment of the block polymer or comb backbone may comprise the same polymer as the membrane bulk (PAN, PVDF),[30,54] or it may be a polymer that adsorbs to the matrix due to favorable van der Waals

https://dx.doi.org/10.1021/acsnano.0c07883
ACS Nano 2020, 14, 16446−16471

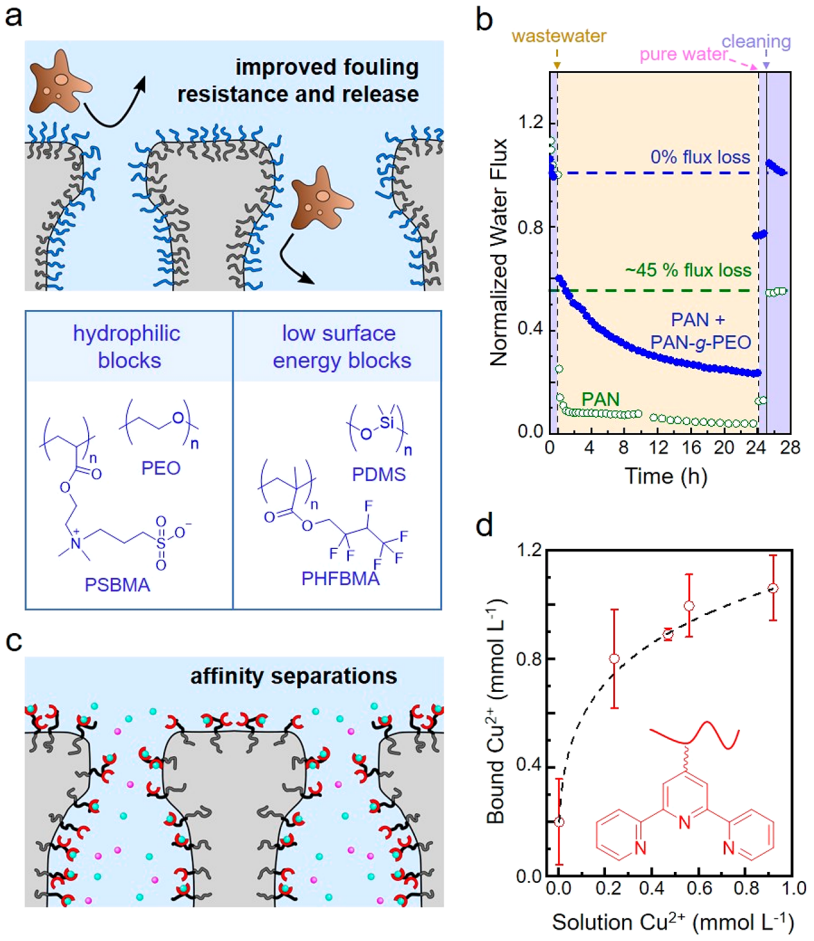

Figure 3. Incorporating a small amount of an amphiphilic block polymer into a homopolymer solution in NIPS results in the surface segregation of the block polymer molecules along the pore walls (a, c). The hydrophobic block (gray) anchors the molecule into the membrane matrix, while the hydrophilic block (blue) extends into water to improve the wettability of the pores. The chemical structures of representative hydrophilic and low surface energy polymers are presented in (a). The effectiveness of such chemistries in improving fouling resistance is demonstrated in (b). By incorporating a surface-segregating PAN-*g*-PEO polymer (closed blue circles) into a PAN membrane (open green circles), the water flux recovery ratio can be significantly improved following exposure to oil refinery wastewater and membrane cleaning. Reproduced with permission from ref 57. Copyright 2004 American Chemical Society. Additionally, surface segregation can be used to promote affinity-driven separations by designing a hydrophilic block that also contains selective binding functionalities (c). This strategy was used to bind aqueous copper ions by functionalizing the PAA block of a surface-segregating PS-*b*-PAA diblock with a terpyridine ligand (d). Reproduced with permission from ref 33. Copyright 2018 American Chemical Society.

interactions (poly(methyl methacrylate) (PMMA)).[55] Common hydrophilic blocks and side chains include polyelectrolytes (polymethacrylic acid (PMAA), poly(acrylic acid) (PAA)),[54] anti-fouling segments (poly(ethylene oxide) (PEO)),[30] and polyzwitterions (poly(sulfobetaine methacrylate))[58] (Figure 3a). These systems have been effective at reducing membrane fouling, where the incorporation of amphiphilic PAN-*g*-PEO comb polymers into PAN membranes resulted in near complete recovery of water flux after oil refinery wastewater filtration and membrane cleaning (Figure 3b).[57] Commercially available PEO-PPO-PEO triblock polymer surfactants (Pluronic or Poloxamer) have also been shown to effectively improve the fouling resistance.[59]

The surface segregation approach can also be extended to non-polar low surface energy segments, such as silicone and fluorinated polymeric materials, that impart foulant release functionalities. However, these polymer segments do not spontaneously migrate to the surface in aqueous coagulation baths due to their incompatibility with water (the most commonly used non-solvent). Therefore, they must be covalently bonded to hydrophilic polymer segments to promote their segregation to the membrane surface. Copolymers containing fouling release segments, such as poly(hexafluorobutyl methacrylate) and polydimethylsiloxane (PDMS), with the previously discussed hydrophilic moieties induces segregation along the membrane surface and pore walls (Figure 3a).[60−63] The low quantities of block polymer required for the surface segregation of amphiphilic or low surface energy polymers offers the potential to improve fouling resistance without significantly increasing costs. The resulting membranes could have potential to advance water treatments processes where fouling resistance is paramount, particularly for MBR.

Beyond fouling resistance and release, surface segregation can also be used to impart functionalities into NIPS membranes, facilitating affinity-driven separations (Figure 3c). For example, polyethylenimine and metal-binding terpyridine ligands attached to PAA-lined pores of PSF/PS-*b*-PAA blends were shown to effectively adsorb heavy metal contaminants (Figure 3d).[33] Continued development of

https://dx.doi.org/10.1021/acsnano.0c07883
ACS Nano 2020, 14, 16446−16471

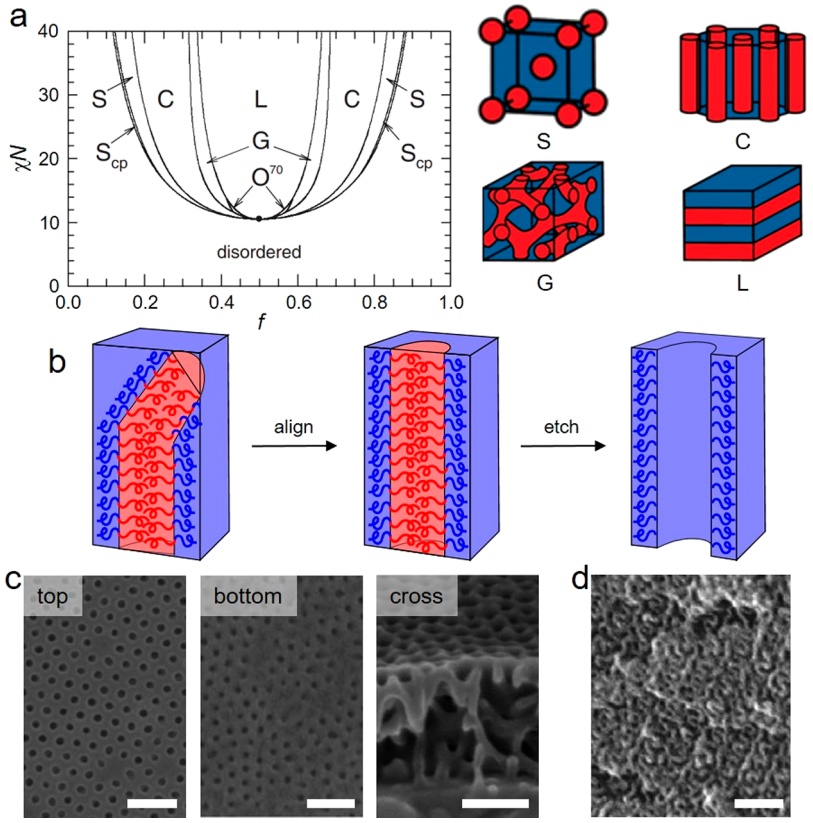

Figure 4. Illustration of block polymer self-assembly and the integration of these nanostructures into porous membranes. A representative phase diagram for diblock polymers is presented in (a) along with cartoon representations of the lamellar (L), double gyroid (G), hexagonally packed cylindrical (C), and spherical (S) morphologies. Phase diagram reproduced with permission from ref 76. Copyright 2009 Springer. Block polymer morphologies reproduced with permission from ref 77. Copyright 2020 American Chemical Society. For anisotropic morphologies, such as hexagonally packed cylinders, additional alignment steps are often required to obtain the continuous domains and pores that are required for water transport (b). This ensures that the pores span the length of the active layer, as demonstrated by SEM images of the top and bottom surfaces of a PS-*b*-PMMA selective layer on a porous PES support layer following solvent vapor annealing and PMMA removal (c). Adapted with permission from ref 23. Copyright 2008 John Wiley & Sons Ltd. Alternatively, a PB-*b*-PDMS block polymer with an isotropic and co-continuous double gyroid morphology eliminates the need for the alignment of anisotropic domains to produce continuous pores (d). Reproduced with permission from ref 78. Copyright 2011 Elsevier. The scale bars correspond to 200 nm in (c) and 100 nm in (d).

functionalized surface segregated layers may further expand the scope of separations capabilities of UF membranes.[35] However, despite the improved fouling resistance of NIPS membranes with surface-segregating block polymer additives, these membranes still exhibit the broad pore size distributions and limited size selectivity that is characteristic of NIPS membranes.

SELECTIVE ETCHING OF SELF-ASSEMBLED BLOCK POLYMERS

Self-assembled block polymers are attractive targets for polymeric UF membranes, as their uniform domain sizes and tunable morphologies are expected to enable more precise separations than is currently possible with NIPS membranes.[3,6,7,15] A conceptually straightforward route to prepare block polymer-based UF membranes is to first cast a solid film and then use the inherent self-assembled nanostructure as a template for pore generation. These membranes can be either free-standing block polymer films or composite architectures, where a thin block polymer selective layer is cast atop a porous substrate (typically a NIPS membrane). Pores are generated by selectively removing (etching) one of the domains, and the pore size is directly related to the initial molar mass of the etchable block.[18,21,22]

Fabricating high-performance UF membranes from solid block polymer thin films requires a basic understanding of the physics governing their self-assembly. Block polymers containing chemically dissimilar blocks exhibit a strong enthalpic drive to phase separate due to unfavorable interactions between the blocks. However, the covalent linkages between these blocks limit segregation to molecular length scales. Consequently, these materials microphase separate at the nanoscale into regularly ordered domains of nearly uniform size (Figure 4a).[13,14,64] The thermodynamic drive to microphase separate is described by the segregation strength, χN, where χ is an interaction parameter that scales inversely with temperature and N is the reference-volume-normalized degree of polymerization. At high values of χN (low temperatures or high molar masses), the enthalpic drive to phase separate dominates, and an ordered microphase separated morphology will be obtained. The symmetry of the morphology is governed by the volumetric ratio of the blocks, with a general transition from lamellae to network phases (gyroid) to cylinders to spheres as the block length asymmetry increases. At lower values of χN (higher temperatures and/or lower molar masses), the

https://dx.doi.org/10.1021/acsnano.0c07883
ACS Nano 2020, 14, 16446−16471

enthalpic drive to phase separate will decrease relative to the energetic considerations associated with the entropic drive to minimize chain stretching. Eventually, this results in a loss of long-range order at the order−disorder transition (ODT) temperature (T_{ODT}).[64,65] For a given block polymer chemistry (and associated χ), this sets a lower practical limit on the attainable pore size, typically in the range of 5−10 nm.[66] There has been much recent activity in pushing the lower limit of block polymer self-assembly to even smaller feature sizes, but these studies have not been translated into membrane technologies.[66−68] Figure 4a presents illustrations of morphologies commonly found in the phase map for an idealized diblock polymer. Related diagrams for real polymers also include contributions from molar mass dispersity and conformational asymmetry (relative flexibilities of the polymer backbones) that will alter the behavior from this idealized state.[69−71] Furthermore, the introduction of additional blocks and non-linear chain architectures can greatly enrich the complexity of the phase diagram, providing access to previously unobserved equilibrium morphologies.[72−75]

Scope of Polymer Chemistries. Block polymers appropriate for use as self-assembled templates in UF membranes must incorporate one domain that can be selectively removed to generate pores without compromising the structure of the remaining matrix-forming block(s). The most commonly used sacrificial blocks are aliphatic polyesters, owing to their facile hydrolysis under mildly basic conditions. In particular, polylactide (PLA) has become ubiquitous in this regard due to its ease of synthesis, widespread availability, and innocuous degradation products.[18,21,22] Other than recent work on poly(propylene carbonate) (PPC),[79] research into the use of aliphatic polycarbonate, polyethers, and other aliphatic polyesters has been limited.

Other chemistries that are not susceptible to hydrolysis have also been used as the pore-forming block, although more involved degradation strategies are often needed. Early work focused on poly(methyl methacrylate) (PMMA) as the etchable block, where pores were generated by plasma etching or UV irradiation.[23,80] Alternatively, selective etching of poly(dimethylsiloxane) (PDMS) has been demonstrated in hydrofluoric acid and tetra-*n*-butylammonium fluoride (TBAF).[78,81,82] Rather than completely removing one block, pore generation can also be achieved by selective extraction of homopolymer diluents. For example, extraction of PEO homopolymer from the poly(4-vinylpyridine) (P4VP) domain of a PS-*b*-P4VP diblock and poly(acrylic acid) from the PEO phase of PS-*b*-PEO diblock generated narrow pore size distributions comparable to systems where one block was completely removed.[83−85] A summary of commonly used etchable blocks and their required etching conditions is provided in Table 2.

Similar to NIPS, selectively etched membranes require a matrix-forming block with a sufficiently high elastic modulus to prevent pore collapse. Lower T_g polymers (such as polybutadiene) can be used, but they require a high degree of cross-linking to exhibit a sufficiently high modulus to stabilize the porous structure.[78,82,88] High-T_g polymers, in contrast, are able to maintain pore integrity without the need for cross-linking; polystyrene (PS) has received significant attention for this reason.[18,21,23,83] A major disadvantage of a glassy and high T_g matrix, like PS, is a lack of toughness, especially when low molar mass blocks are used (*e.g.*, in attempts to attain small pore sizes). Toughness can be improved by incorporating a low T_g polymer, such as polyisoprene or polybutadiene, into a multiblock architecture that combines the rubbery nature of the low T_g block with the rigid nature of the high T_g block. This strategy has resulted in a ∼40-fold increase in strain at break for PS-*b*-PI-*b*-PS-*b*-PLA[22] compared to PS-*b*-PLA.[89]

Table 2. Commonly Used Etchable Blocks and Their Respective Etching Procedures

Etchable Polymer	Chemical Structure	Etching Mechanism	Etching Conditions for Thin Films
PLA	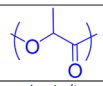	base-mediated hydrolysis	2 M NaOH 25 °C, 1-3 h[86,87]
PDMS		TBAF; HF	1 M TBAF, 25 °C;[82] 12 M HF, 0 °C, 2 h[78,81]
PMMA	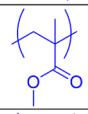	UV irradiation followed by acetic acid rinse; plasma etching	253 nm UV for 3 h acetic acid 1 h, 25 °C;[23] Ar/O_2 plasma, 1-5 min[80]
PEO	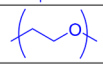	acid-catalyzed hydrolysis	14 M HI, 60 °C, 5 days[85]
PPC	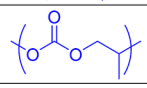	base-catalyzed hydrolysis	2 M NaOH 80 °C, 1 h[79]

Domain Alignment of Anisotropic Ordered Morphologies. An ideal block-polymer UF membrane has continuous and uninterrupted pores that span the entire length of the selective layer to achieve high water permeability. However, anisotropic cylindrical morphologies typically exhibit polycrystalline microstructures with domains that are misoriented at grain boundaries, disrupting pore continuity and inhibiting water transport (Figure 4b).[18,21,90] Therefore, careful design of the coating parameters or various alignment strategies are often required to obtain continuous pores.

In some cases, spontaneous orientation of cylindrical domains perpendicular to the film surface can be achieved through careful selection of the coating parameters.[18,21,90] Dissolving the block polymer mitigates unfavorable segment−segment interactions, lowering the segregation strength and causing the block polymer to disorder. Under solvent evaporation, the segregation strength effectively increases toward the melt segregation strength (*i.e.*, the segregation strength in the absence of solvent), creating a thermodynamic driving force for microphase separation.[90,91] Domains nucleate at the film−air interface and anisotropically grow across the film thickness along the concentration gradient. Rapidly drying a film increases the thermodynamic drive for domain growth more than it decreases the mobility of the polymer chains, resulting in the desired perpendicular orientation. Conversely, slower rates of solvent evaporation promote domain growth parallel to the film surface due to a driving force that increases slower than the decrease in chain mobility.[90] For the commonly used PS-*b*-PLA system, these parameters are well-documented and have been incorporated into UF membrane fabrication to varying degrees of success.[21,22,90] However, these parameters are highly system dependent, and identifying similar guidelines for different polymer chemistries requires extensive experimental screening.

If needed, the block polymer film can be thermally annealed above its highest T_g for glassy polymers or melting temperature (T_m) for semi-crystalline polymers, where misoriented domains have sufficiently high mobility to rearrange into a

https://dx.doi.org/10.1021/acsnano.0c07883
ACS Nano 2020, 14, 16446−16471

more thermodynamically favorable orientation. Domain orientation is highly dependent upon the relative interfacial (polymer−substrate) and surface (polymer−air) energies of the blocks.[92−94] Perpendicular alignment occurs when the interfacial and surface energies of the constituent blocks are nearly identical or when the film thickness is smaller than the periodicity of the self-assembled domains.[92] However, block polymers with significantly different interfacial and surface energies orient parallel to the surfaces, resulting in an unsuitable morphology for UF membranes.[95−97] For example, cylindrical domains which are perfectly oriented parallel to the film surface will produce discontinuous pores upon etching, where water flow is interrupted by the non-porous and typically hydrophobic matrix. The utility of thermal annealing can be limited by the long times (several hours) and high temperatures (~200 °C) required, which can potentially degrade the block polymer or disrupt the pores in the support layer.

Instead of heating above T_g or T_m, exposure to solvent can lower the thermal transition below room temperature—a process termed solvent vapor annealing (SVA).[98] The polymer chains swell upon exposure to a non-preferential or slightly preferential solvent vapor, resulting in an increase in film thickness and chain mobility.[90,98,99] Solvent mediates the unfavorable enthalpic interactions between the different blocks, lowering χN. Additionally, solvents that are slightly preferential for one block effectively increase the relative volume occupied by that block, and thus the volume fraction, f. The increased mobility of the swollen chains facilitates reorganization into the thermodynamically favored (or potentially metastable) morphology corresponding to the decreased χN and the effective f.[98,99]

The morphology of the non-swollen state and the overall degree of swelling determine the swollen state morphology. Rapid drying kinetically traps the morphology that can be achieved by traversing a lower energy barrier, potentially enabling perpendicular orientation even when it would be otherwise energetically unfavorable.[98] In contrast, slow solvent removal results in the nucleation and growth of domains from the film surface, resulting in domains aligned along the most energetically favored orientation.[98]

The significant process dependence of SVA represents a major challenge. Expensive and time-intensive optimization must be taken for each configuration of solvent, polymer, and apparatus. Additionally, the need for specialized equipment limits the commercial production of large and cost-effective membranes. For composite block polymer membranes, the solvents may also plasticize the porous polymeric support layer and adversely affect its mechanical integrity and porosity. Support layer plasticization can be mitigated by transferring the block polymer selective layer from a solvent-stable sacrificial substrate onto a porous support after SVA. This has been successfully demonstrated by using SVA to generate perpendicularly oriented cylinders in a PS-*b*-PMMA film on a solvent-stable Si substrate and then transferring this film onto a porous PES substrate (Figure 4c) to produce a membrane with a high water permeability, 200 L m^{-2} h^{-1} bar^{-1}, and complete virus rejection.[23]

Magnetic fields have recently received interest as an alternative to quickly align block polymer domains without the use of solvents.[100−103] Perpendicularly oriented cylindrical pores have been obtained in films of a brush block polymer composed of a selectively etchable polylactide block and a polynorbornene block with side chain liquid crystalline mesogens.[102,104] However, films of both of these polymers were too thick to function as viable UF membranes. Successful incorporation of field-based alignment at membrane relevant size scales faces practical hurdles due to the technological challenge of overcoming surface interactions in films that are thin enough to serve as UF selective layers.[103] Furthermore, highly specialized equipment is required to achieve sufficiently strong magnetic fields—typically in the range of several Tesla.

Utilization of Isotropic Ordered Morphologies. Morphologies that inherently possess co-continuous and interconnected domains eliminate the need for complicated alignment processes. The ordered network phases between the lamellar and cylindrical regions of the phase diagram have received the most attention for this purpose, particularly the gyroid morphology.[78,81,82] However, applications of the gyroid morphology have been limited by the relatively narrow region of phase space (defined by χN and f) where this morphology is typically observed.[105] Targeting these domains often requires precision synthetic methods, such as anionic polymerization, which significantly increase the cost of polymer synthesis. Complex polymer architectures (multiblocks, miktoarm stars, *etc.*) and high dispersity blocks can slightly expand the thermodynamic stability of the gyroid phase but can also require complex synthetic techniques.[70,106,107] Free-standing films of cross-linked PB-*b*-PDMS with a gyroid morphology have been used as UF membranes (Figure 4d), but these thick films (25 μm) displayed relatively low water permeabilities, ~10 L m^{-2} h^{-1} bar^{-1}.[78,81] To the best of our knowledge, composite membranes with a thin gyroid selective layer have not been reported, possibly due to difficulties in nucleating this morphology in very thin films (~100 nm).[108,109]

The inverse cylinder morphology (where the etchable block forms the matrix rather than the minority phase) is another potential option for continuous pores. Unlike the standard cylinder arrangement, placing the etchable block in the majority domain can result in continuous pores without the need to orient the minority cylindrical phase.[110] Based on the high volume fraction occupied by the etchable block ($f_{etchable}$ ≈ 0.65−0.8), higher porosities than cylinders with an etchable minority phase ($f_{etchable}$ ≈ 0.2−0.35) are attainable. However, upon etching, the matrix-forming domains are discontinuous, so interdomain cross-linking is required to prevent pore collapse. Such a strategy has been employed in the fabrication of NF membranes from polymerizable surfactants.[110] Similar approaches have yet to be investigated for block polymer systems for UF membranes, but they may be a promising area for future research.

Utilization of Isotropic Disordered Morphologies. Instead of equilibrium ordered morphologies, recent work in the field has focused on kinetically trapped disordered morphologies with co-continuous microphase separated domains.[86,87,111−113] These systems generally exhibit advantages similar to those of the gyroid morphology (inherently continuous domains without the need for alignment), while being accessible across a wider range of block polymer compositions. Owing to their self-assembled domains, these disordered morphologies exhibit narrow pore size distributions comparable to equilibrium ordered morphologies. As these disordered morphologies are non-equilibrium states under typical UF use conditions, cross-linking reactions or thermal processing techniques are required to kinetically trap these states prior to use.[86,111]

https://dx.doi.org/10.1021/acsnano.0c07883
ACS Nano 2020, 14, 16446−16471

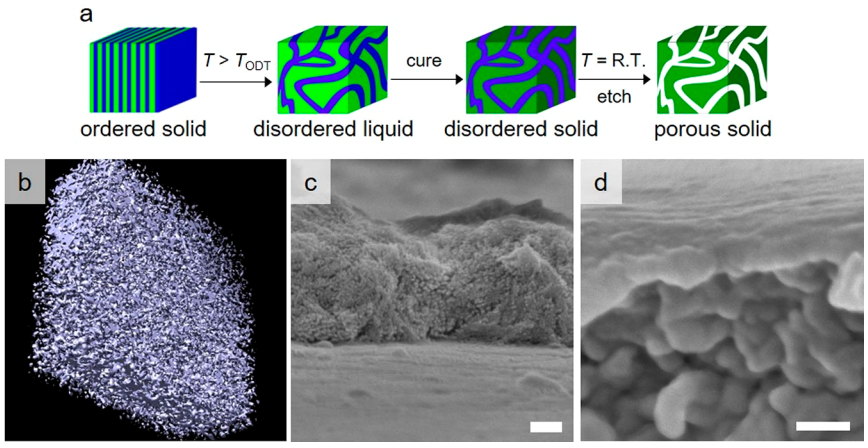

Figure 5. Illustration of the process used to kinetically trap disordered state composition fluctuations for the purpose of generating co-continuous pores (a). The three-dimensional connectivity of these pores has been demonstrated by a transmission electron microtomographic reconstruction of a cross-linked and etched P(S-*s*-GMA)-*b*-PLA diblock (b). Reproduced with permission from ref 86. Copyright 2017 American Chemical Society. The use of the disordered state also helps facilitate co-casting techniques that can be integrated with existing NIPS processes, as has been demonstrated for dual-layer membranes comprising a kinetically trapped P(MMA-*s*-S)-*b*-PLA selective layer and a PSF support layer (c). Reproduced with permission from ref 87. Copyright 2019 American Chemical Society. The block polymer-derived selective layers of these composite membranes maintain the bicontinuous pore structure observed in bulk monoliths across the entire thickness, where the pores generated from a photocured P(S-*s*-GMA)-*b*-PLA were observed to span the entire thickness of the selective layer (d). Reproduced with permission from ref 119. Copyright 2020 American Chemical Society. The scale bar corresponds to 200 nm in (c) and 100 nm in (d).

One kinetic trapping strategy is polymerization-induced microphase separation (PIMS).[111,114] In PIMS, a polymer end-functionalized with a chain transfer agent (CTA) appropriate for reversible addition−fragmentation chain-transfer (RAFT) polymerization is dissolved in a mixture of mono- and difunctional monomers. A polylactide macro-chain transfer agent (PLA-CTA) dissolved in a monomeric mixture of styrene and divinylbenzene (DVB) has been used extensively in this approach.[111,114] Thermal[111,114,115] or UV initiation[116] results in the RAFT copolymerization of the monomers to form a cross-linked block polymer. As the block polymer grows (N increases), the segregation strength increases, inducing microphase separation. The cross-linking reaction kinetically traps the incipient microphase separated domains in a disordered and co-continuous state before the block polymer can order into its thermodynamic equilibrium morphology.[111,114] Following removal of the etchable domains, a continuous network of uniformly sized pores can be obtained. Generally, the water permeabilities of these films are very low, ∼0.5 L m^{-2} h^{-1} bar^{-1}, due to the large film thickness, ∼300 μm.[111] Thinner films, ∼100 nm to 1 μm, are required for obtaining water permeabilities comparable to commercial UF membranes with similar average pore sizes, but the relatively high volatility of typical liquid monomer reaction mixtures has hindered this goal.

To address the processing challenges inherent to PIMS, our group has recently developed a method to obtain similar morphologies from preformed block polymers amenable to solution processing.[86,87,113,117] Above the order−disorder transition temperature (T_{ODT}), composition fluctuations in block polymer melts result in a disordered, yet microphase-separated, morphology that resembles spinodal decomposition.[65,118] This morphology exists at a much smaller length scale than in immiscible polymer blends, resulting in inherently co-continuous domains with sizes appropriate for UF membranes. Kinetic trapping of disordered state composition fluctuations requires an ordered and chemically reactive block polymer that can be heated into the disordered state and subsequently cross-linked (Figure 5a).[86,113] Stable pores can then be generated by selectively removing the uncross-linked, sacrificial domain (Figure 5b). Polymers that contain pendant epoxide or unsaturated moieties, such as poly(glycidyl methacrylate)[86,87] and polybutadiene,[113] have proven successful for introducing latently cross-linkable functionalities into the matrix. Epoxide-containing domains are cured using thermal[86] or photoacid generators,[87] while unsaturated systems can be cured through a radical process.[113] Thermal quenching of high T_g polymers can also be used to trap the fluctuating disordered state by rapidly quenching the block polymer from above the T_{ODT} to below T_g.[117] The low mobility of the chains in the glassy state and the relatively high modulus preserves the disordered and co-continuous network of pores, and has allowed for comparable porosities to the cross-linked systems.[117]

Film Casting Strategies. A number of different strategies have been employed to fabricate etchable block polymer UF membranes. The simplest method involves solvent casting free-standing films of block polymer from solution.[24,26,78,81] Upon solvent evaporation, a solid film comprising solely block polymer is obtained. While this strategy does not require any elaborate processing steps and is thus easy to scale, relatively thick films (on the order of hundreds of micrometers) are needed to provide the mechanical robustness necessary for hydraulic pressure-driven membrane operations. Due to their small pores, these thick films have low water permeabilities that are generally not competitive with existing NIPS membranes, despite their improved size selectivity.[26,78]

Thinner (yet still mechanically robust) block polymer films would be highly advantageous for improving water permeability in a practical manner. One strategy is to fabricate composite membranes comprising a thin block polymer selective layer that imparts high size selectivity on top of a thicker macroporous support layer (often a NIPS membrane) that imparts high water permeability and mechanical robust-

https://dx.doi.org/10.1021/acsnano.0c07883
ACS Nano 2020, 14, 16446−16471

ness. The most direct route toward such a composite membrane is to directly coat a dilute block polymer solution atop a porous NIPS membrane.[18,21,22,79] The pores of the support layer are often filled with water (or another liquid that is immiscible with the casting solvent) prior to coating the block polymer film to prevent infiltration into the support.[18,21] Additionally, the support layer must be resistant to the casting solvent used for the block polymer layer. Composite membranes can also be heated to cross-link the block polymer selective layer and increase its mechanical robustness or kinetically trap a non-equilibrium morphology (Figure 5c).[86,87,113] However, high temperatures, harsh conditions, and long curing times are often needed for cross-linking reactions, which may lead to densification of the support layer pores.

Blade coating techniques are particularly attractive for the block polymer solution due to the simplicity and scalability of these processes. However, the literature in this area has revealed challenges associated with fabricating block polymer layers that are thin enough (less than approximately 1 μm) to achieve a high water permeability.[18,79] Conversely, spin coating has resulted in the fabrication of sub-100 nm block polymer selective layers with significantly improved water permeability, but spin coating is difficult to implement at the scale of industrially relevant membrane modules.[21,22] Rather than directly coating onto an existing porous membrane, it is also possible to first coat a very thin (sub-100 nm) block polymer film on top of a non-porous sacrificial substrate and then transfer it onto a NIPS membrane.[22,23] Salt discs[22] and silicon wafers[23] are the most commonly used sacrificial substrates, as they are dissolved in water and hydrofluoric acid, respectively, to yield a thin and free-standing block polymer film. Sacrificial substrates often have high solvent and thermal stabilities as compared to NIPS membranes, enabling the use of annealing and postfunctionalization processes that might compromise the integrity of a porous polymeric support.[23] However, the process of transferring a large film is extremely challenging, which limits the viability of this approach.

Recent research has focused on co-casting block polymer and a homopolymer solutions to produce composite membranes in a single process. In a recent proof of concept, a dilute solution of a P(MMA-*s*-S)-*b*-PLA diblock was directly coated on top of a solvent-swollen polysulfone support layer.[119] Subsequent immersion of the film in an ice water coagulation bath precipitated the polysulfone layer by NIPS and kinetically trapped the fluctuating disordered state of the block polymer, resulting in a composite membrane (Figure 5d) with a high water permeability of ~150 L m^{-2} h^{-1} bar^{-1} and highly selective pores of approximately 15 nm in diameter.[119] This process can be realized at a large scale using existing industrial membrane fabrication infrastructure. Further refinement is expected to enable roll-to-roll production of highly selective membranes competitive with commercial technologies in terms of water permeability, scalability, and cost.

SELECTIVE SWELLING OF SELF-ASSEMBLED BLOCK POLYMERS

An emerging method of fabricating UF membranes from self-assembled block polymers uses the selective solvent swelling of one block to generate pores.[120,121] Like the previously discussed method of selective degradation, selective swelling-induced pore generation is performed on solid block polymer films that are self-assembled into their thermodynamically favored morphology. However, instead of chemically etching one domain, pores are produced through the volumetric expansion of one block in the presence of a highly selective solvent.[120,121] This method eliminates the formation of degradation byproducts inherent to selective etching and simplifies membrane production. One of the major advantages of the selective swelling strategy is that the swellable polar block remains intact in the final membrane, which can result in a hydrophilic surface and pore walls that improve the wettability and fouling resistance of the membrane.[16,122] Additionally, pore generation can proceed significantly faster than for selectively etched membranes, notably producing uniform pores in less than 1 min using microwave heating.[123]

Scope of Polymer Chemistries. Selective swelling-induced pore generation requires the constituent polymer blocks to have significantly different polarities. This ensures that the solvent is highly preferential for only one block and non-preferential (or highly unfavorable) for the other(s). An early report of selective swelling induced pore generation in UF membrane fabrication used a PS-*b*-PMMA diblock to produce UF membranes with high water permeabilities and narrow pore size distributions.[124] Contemporary efforts have focused heavily on PS-*b*-P2VP diblocks due to their lower water contact angle and improved pore wettability post-swelling.[19,122,125] The hydrophilicity has been further improved by employing PS-*b*-PEO diblocks, as the presence of the hydrophilic PEO chains along the membrane surface and pore walls imparts a high degree of fouling resistance.[16,126,127]

Recent research has focused on replacing the brittle PS block with a mechanically robust PSF block (*e.g.*, PSF-*b*-PEO) in an effort to make a more commercially relevant membrane.[121,128,129] Produced by step growth synthesis, these PSF-containing block polymers have an inherently higher molar mass dispersity than block polymers synthesized using controlled chain-growth polymerization. However, the effect of this high dispersity on the pore size distribution has received little attention. Future research efforts are likely to continue the development of block polymers chemistries similar to those that are currently used in membrane fabrication.

Detailed Mechanistic Description. A definitive mechanistic understanding of selective swelling-induced pore generation is still unclear, but the current hypothesis based on existing literature will be discussed for the well-studied PS-*b*-P2VP diblock polymer in ethanol (Figure 6a).[120,122] Ethanol is highly selective for the P2VP block, yet a very poor solvent for the PS matrix block. Consequently, ethanol partitions into the P2VP block almost exclusively, while potentially slightly plasticizing the PS block. As the P2VP chains swell, an osmotic driving force causes them to stretch and deform. This results in an increase in the film thickness to accommodate the volumetric expansion of the swollen chains, as confirmed by spectroscopic ellipsometry (Figure 6b).[120,122] Swelling is typically performed at elevated temperatures to facilitate some plastic deformation of the PS matrix (the T_g of PS decreases from ~100 °C in bulk to ~85 °C in the presence of ethanol).[120,121,130] However, the swelling temperature is still typically below the T_g of PS in the presence of ethanol.[122] Therefore, deformation of the PS matrix is expected to occur locally at the domain interface, as mixing between the highly swollen P2VP block and the PS block may further depress T_g near the block junction.[131] When the swollen film is removed from the selective solvent, the PS chains are believed to immediately vitrify and the previously swollen P2VP chains

https://dx.doi.org/10.1021/acsnano.0c07883
ACS Nano 2020, 14, 16446−16471

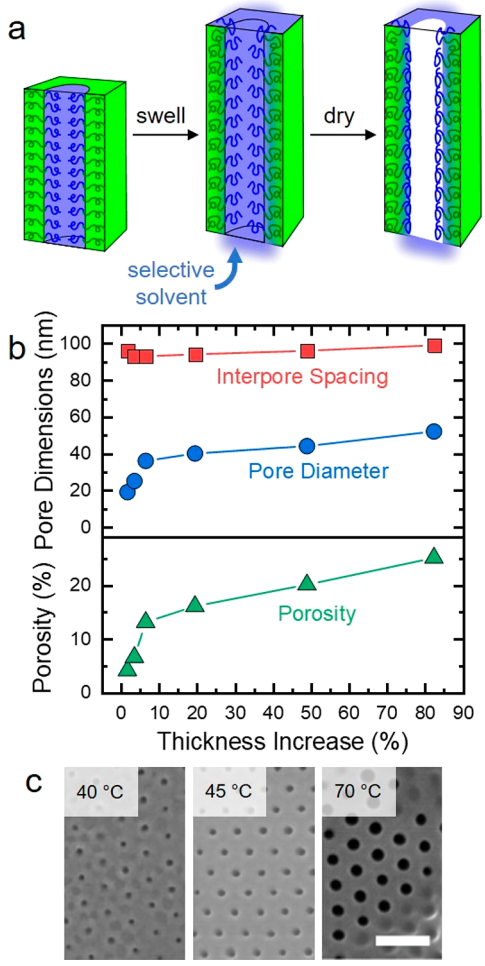

Figure 6. Illustration of selective-swelling-induced pore generation (a). This proposed mechanism has been supported by the strong correlation between the increase in film porosity (green triangles) and pore diameter (blue circles) with the increase in film thickness upon swelling PS-*b*-P2VP (b).[120] Conversely, the interpore spacing (red squares) remains constant, indicating that swelling is confined in the lateral direction. The effect of swelling temperature at a constant swelling time for a PS-*b*-P2VP diblock in ethanol is presented in (c). Reproduced with permission from ref 122. Copyright 2013 American Chemical Society. The scale bar in (c) corresponds to 200 nm. Generally, higher swelling temperatures (40, 45, and 70 °C from left to right) result in larger pores due to an increased degree of swelling.

collapse against the glassy matrix. The collapsed P2VP chains are enriched on the membrane surface as well as the pore walls, as evidenced by a decrease in the water contact angle of the films post-swelling.[124] The volume that was previously occupied by ethanol in the P2VP domains is converted into pores, as supported by the strong correlation between increased film thickness and increased porosity and pore size. However, interestingly the measured porosity is lower than expected based on the volumetric expansion of the film, suggesting that some of the swollen volume is not converted into accessible pores. Higher swelling temperatures increase the mobility of the PS chains, facilitating plastic deformation and greatly increasing the degree of swelling.[122] Therefore, adjusting the swelling time and temperature can tune the average pore size and overall film porosity (Figure 6c).[122]

Film Casting Strategies. Both free-standing[128,129,132] and composite membranes[19,124,125,133,134] have been reported, but the higher water permeabilities and lower materials requirements of composite membranes are preferred. Melt extrusion of UF membranes from PSF-*b*-PEO has also been reported, where microwave heating the extrudate in the solvent bath can significantly reduce the time required for pore generation from several hours to several seconds.[135] While this process has been primarily applied to thick films (ca. 50 μm) thus far, it is a promising strategy for practical membrane production, provided that it can be extended to sufficiently thin films (ca. 100 nm).[123]

Domain Alignment and Morphological Control. As discussed for selectively etched block polymer UF membranes, the self-assembled domains must be converted into continuous pores. One notable feature of the selective swelling mechanism is that cylindrical domains do not necessarily have to be perpendicularly aligned through the thickness of the film to obtain continuous pores. Instead, randomly oriented cylindrical domains merge and interconnect to form bicontinuous pores upon the selective swelling of PS-*b*-P2VP.[19,134,136] This facilitates the fabrication of highly permeable UF membranes without having to execute complicated alignment procedures. Bicontinuous structures with a percolating pore network can also be produced by selectively swelling disordered block polymers that still exhibit locally microphase separated domains, as has been demonstrated for PSF-*b*-PEO.[128,129]

For certain applications, it may be advantageous to align cylindrical domains to reduce pore tortuosity by using the previously discussed techniques. Continuous pores have been reported for cylinders with both parallel[137] and perpendicular[126] orientations in PS-*b*-P2VP, offering the possibility of tuning the pore topology from slits to cylinders, respectively. This may be an interesting platform for examining the relationship between pore morphology and water transport at the nanoscale, informing the development of transport models specifically tailored toward UF and NF.

EVAPORATION-INDUCED SELF-ASSEMBLY FOLLOWED BY NON-SOLVENT-INDUCED PHASE SEPARATION

One of the most promising fabrication strategies for block polymer UF membranes combines the principles of block polymer thermodynamic self-assembly with traditional non-solvent-induced phase separation—a process termed evaporation-induced self-assembly followed by non-solvent-induced phase separation (SNIPS).[7,20,138] The presence of solvent in SNIPS drives the block polymer molecules to self-assemble into micelles rather than the previously discussed morphologies in solid films. The SNIPS process follows a similar protocol as traditional NIPS.[20] Briefly, a concentrated block polymer solution is cast into a film and immersed in non-solvent after a short evaporation time to induce phase separation and pore formation. By virtue of this similarity, the SNIPS process should be readily integrated into existing industrial coating methods, potentially enabling commercially viable roll-to-roll membrane fabrication.[7,139] In comparison to NIPS membranes, the microphase separated nanostructures inherent to block polymers result in more regular and uniform surface pores and enable more precise solute separation.

Like NIPS membranes, SNIPS membranes exhibit an asymmetric and integral architecture with a thin active layer that gradually transitions into a thicker and more porous

https://dx.doi.org/10.1021/acsnano.0c07883
ACS Nano 2020, 14, 16446−16471

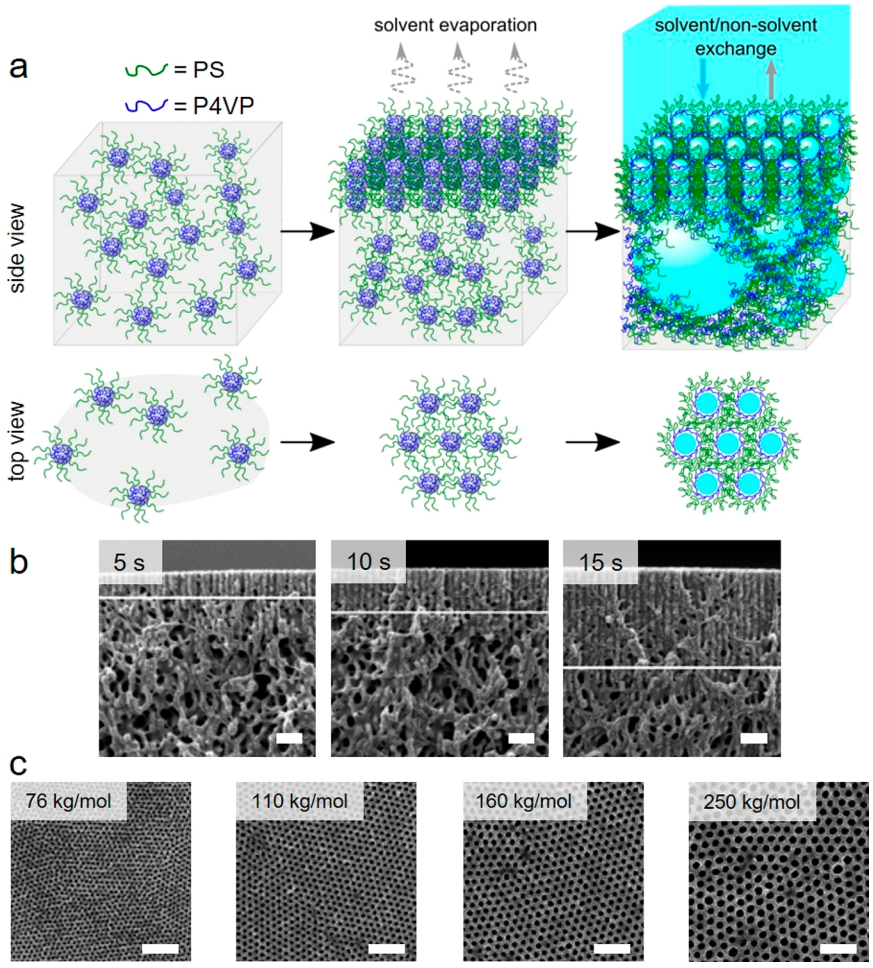

Figure 7. SNIPS for the well-studied PS-*b*-P4VP system in DMF/THF. In the putative SNIPS mechanism (a), a concentrated solution of PS-*b*-P4VP in DMF/THF self-assembles into micelles composed of a P4VP core (blue) and a PS corona (green). After casting a film, a disordered packing of micelles is initially obtained. A short solvent evaporation step drives the micelles to pack into an ordered hexagonal arrangement of cylindrical channels at the film−air interface. Immersing the film into non-solvent exchanges the casting solvent for the non-solvent, resulting in the precipitation of the polymer into a solid film with P4VP-lined pores supported by a solid PS matrix. The development of the cross-sectional morphology for a PS-*b*-P4VP membrane with increasing evaporation time is presented in (b). Reproduced with permission from ref 164. Copyright 2017 John Wiley & Sons Ltd. Active layer thickness increases with the evaporation time due to increased intermicellar interactions that drive cylinder growth. The tunability of the average pore size is demonstrated in (c) for a PS-*b*-P4VP system. Reproduced with permission from ref 165. Copyright 2014, published by The Royal Society of Chemistry. Increasing the molar mass of the block polymer results in a larger average pore size. The scale bars in (b) and (c) correspond to 200 nm.

substructure.[138] In effect, both the selective and the support layers are composed of block polymer in SNIPS. Such an integral structure eliminates the need to coat a separate block polymer layer on top of a porous support, significantly simplifying the coating process. This architecture also guarantees that the small pores that actively separate the targeted contaminants in the selective layer are well-connected to the much larger pores in the membrane substructure. High water permeabilities can thus be obtained without having to orient the domains, in direct contrast to ordered block polymer solid films. The ultimate membrane properties are highly dependent upon the choice of block polymer chemistry and composition, solution concentration, evaporation time, and solvent.

Scope of Polymer Chemistries. In general, the block polymers used in SNIPS contain a polar block and a non-polar block. The non-polar block forms the membrane matrix, and typically PS has been used due to its easy synthesis and high T_g. The SNIPS mechanism allows flexibility in the choice of the polar block, enabling membrane properties (*e.g.*, pore size, stimuli responsiveness, and fouling resistance) to be precisely tailored toward the targeted application. The most highly studied and arguably most mature system is PS-*b*-P4VP. However, many other polymers have been successfully used for the polar block, including poly(dimethylacrylamide),[140−143] poly(2-vinylpyridine),[144] poly(2-hydroxyethyl methacrylate),[145,146] and poly(ethylene oxide).[147,148] Including a low T_g end block (such as isoprene) can produce more mechanically robust membranes, with PI-*b*-PS-*b*-P4VP membranes displaying toughness values 3 times higher than those of PS-*b*-P4VP.[149] Triblock polymers have also been used to introduce more hydrophilic chemistries, such as PEO[150] and PAA,[142] into the block polymer to improve fouling resistance.

One intriguing feature of using P4VP-containing block polymers is that the pore walls are lined with pyridine moieties. These pyridine groups can serve as a reactive handle for pore wall functionalization, facilitating the introduction of cysteine,[17] dopamine,[17,151,152] and graphene oxide[153] to improve

https://dx.doi.org/10.1021/acsnano.0c07883
ACS Nano 2020, 14, 16446−16471

fouling resistance and bactericidal properties. Additionally, reaction of the pyridine groups with either methyl iodide or propane-1,3-sultone results in cationic or zwitterionic pores, respectively, which can be used to selectively bind charged organic dyes with sizes of ∼1 nm, which would otherwise be too small to remove by UF.[34]

P4VP has a pK_a of 4.6, resulting in the protonation of the pyridine moieties at lower pH.[154] These protonated chains swell in water, constricting the pores and resulting in pore sizes below 5 nm.[154,155] Pore sizes below 10 nm are otherwise difficult to obtain from PS-*b*-P4VP, as a sufficiently high molar mass is needed to obtain well-structured pores.[156] Additionally, this pH-responsiveness allows for the possibility of pore gating.[155] However, in most applications, variability in pore size is disadvantageous and results in an undesirable decrease in water permeability at low pH. For such applications, PEO has been shown to result in pore sizes that are significantly more stable across a range of pH than P4VP.[147] Furthermore, the hydrophilicity of PEO inherently improves the fouling resistance of these membranes without the need for pore wall functionalization.[147,148]

An emerging chemistry for use in SNIPS membranes replaces the P4VP block with poly(*N*,*N*-dimethylacrylamide) (PDMA).[140,141,143] Treatment of PI-*b*-PS-*b*-PDMA triblocks with concentrated acid hydrolyzes the PDMA block to form poly(acrylic acid) (PAA).[140,142,143,157,158] The acrylic acid groups are largely deprotonated at neutral pH (pK_a ≈ 4.5), resulting in negatively charged chains that swell into the pores to reduce repulsive interactions. Consequently, effective pore sizes as small as ∼1 nm can be obtained at neutral pH, potentially enabling these membranes to be used in size-selective NF.[140,143] Below pH ∼3.5, the acrylic acid groups are largely protonated and collapse against the matrix, increasing the pore size to the UF range.[142] Similar features have been obtained by blending PS-*b*-PAA into a PS-*b*-P4VP casting solution.[159] Additionally, PAA-containing SNIPS membranes have been shown to strongly and selectively bind Cu^{2+} which may enable heavy metal removal in addition to traditional UF separations.[33,140]

Detailed Mechanistic Description. The precise membrane formation mechanism for SNIPS is complex, due to its strong dependence on the selected casting parameters, and the overall mechanism is not fully settled. The two most widely studied systems, PS-*b*-P4VP in DMF/THF and PI-*b*-PS-*b*-P4VP in DOX/THF, will be examined in detail here as representative examples. To understand the entire SNIPS mechanism for PS-*b*-P4VP in DMF/THF, it is critical to first establish the self-assembly of the block polymer molecules in the casting solution. Based on their solubility parameters, DMF is a preferential solvent for P4VP and THF is a relatively neutral solvent for both PS and P4VP.[160] These purely enthalpic considerations suggest that the P4VP block will form the corona to minimize less favorable PS-solvent interactions.

However, typical diblocks used in SNIPS membranes are highly asymmetric, containing approximately 65−85 wt% PS.[20,138] Packing these longer PS chains into the micelle core requires a large degree of entropically unfavorable chain stretching.[161,162] Since DMF is a theta solvent for PS rather than a very poor solvent, the enthalpic cost of exposing the PS chains to solvent is lower than the entropic cost of packing these chains into the micelle core. Therefore, it is expected to be thermodynamically favorable to form a spherical micelle with a PS corona and a P4VP core (Figure 7a).[163] Small angle neutron scattering (SANS) experiments of representative solutions support this hypothesis.[162] Contrast matching the P4VP block of PS-*b*-P4VP to DMF made the P4VP domains "invisible" to the incident neutron beam, and an almost complete disappearance of the intermicellar scattering was observed,[162] clearly suggesting that the micelles comprise a solvent-swollen spherical P4VP core that is surrounded by a PS corona in DMF.[163]

After this solution is cast into a film, solvent evaporation primarily occurs at the film−air interface, increasing the local polymer concentration and thus the micelle−micelle interactions. This causes the initially disordered micelles to first coalesce and then arrange into a regularly ordered packing in the surface layer (Figure 7a).[166−168] The structure of this packing is highly dependent upon the choice of solvent, polymer composition, and concentration. For PS-*b*-P4VP in DMF/THF, grazing incidence small-angle X-ray scattering (GISAXS) experiments support a transition from a disordered packing of spherical micelles at the surface to an ordered hexagonal packing with increasing polymer concentration, representing the expected concentration evolution upon film drying.[160,166,167] Solvent evaporation also creates a concentration gradient in the direction normal to the film−air interface that causes the initially spherical micelles to coalesce into perpendicularly oriented cylindrical channels at the film surface (Figure 7b).[164,166,167] Below the film−air interface, solvent evaporation is significantly slower, resulting in a lower concentration of micelles in the substructure. These micelles remain loosely packed in a disordered arrangement.[163,167]

After the evaporation step, the P4VP cores of the cylindrical channels at the film surface remain slightly swollen in solvent.[162] When the film is immersed in water, there is an influx of non-solvent into the P4VP cores (Figure 7a).[139,167] The volumetric expansion caused by the solvent/non-solvent exchange is accommodated by the concomitant contraction of the PS chains in the corona to fill the interstitial space between the micelles.[163] The coalescence of these PS chains physically traps the morphology and prevents further coarsening.[163] Removal of the non-solvent generates uniformly sized surface pores lined by P4VP. The lower concentration and looser micelle packing below the film surface results in a different substructure morphology. In the substructure, pore formation follows the mechanism of traditional NIPS membranes (Figure 2), forming larger pores and a more disperse size distribution.[160,163,167] Due to the concentration gradient that develops during solvent evaporation, there is a gradual transition from the small and uniform pores at the film surface to the large and irregular pores in the substructure.[169] Consequently, these membranes exhibit an integral and asymmetric structure with a thin active layer on top of a thicker support layer.

While the SANS data supporting the described mechanism is compelling, the overall mechanism regarding micelle structure and pore formation in SNIPS remains to be fully established. An alternative mechanism has been proposed, where PS forms the micelle core and P4VP forms the micelle corona due to their respective interaction strengths with DMF/THF.[170] This mechanism was supported by electron microscopy of copper-incorporated micelles and the subsequent membranes, with copper forming complexes with P4VP during membrane formation.[170] In this interpretation, the micelles would still coalesce as solvent evaporates after casting the film. However, P4VP-lined pores would form in the interstitial space between

https://dx.doi.org/10.1021/acsnano.0c07883
ACS Nano 2020, 14, 16446−16471

the micelles upon immersion in water, rather than in the micelle core as we have depicted in Figure 7.

The average pore size at the surface can be rationally tuned by adjusting the molar mass of the PS-*b*-P4VP block polymers (Figure 7c).[165] Additionally, the evaporation time strongly influences the size and regularity of the membrane surface pores and the active layer thickness (Figure 7b).[20,138,149,164] For short evaporation times, the surface layer will be highly swollen, and the micelles will have not yet packed into a regularly ordered arrangement.[149] These membranes closely resemble NIPS membranes and have an irregular arrangement of surface pores with a broad size distribution. Longer evaporation times improve the ordered packing of the micelles at the film surface, resulting in progressively smaller and more regularly arranged pores in the active layer. However, very long evaporation times prevent the solvent/non-solvent exchange required for pore generation, resulting in a non-porous surface that is undesirable for UF membranes.

Chemically similar triblock polymers containing a poly(isoprene) end block (PI-*b*-PS-*b*-P4VP) have also received significant attention, as the rubbery PI block can improve upon the mechanical robustness of PS-*b*-P4VP membranes.[149] These triblock systems are commonly cast from DOX/THF mixtures using similar strategies to those previously discussed for diblocks.[149,154,171,172] While the overall mechanism is generally similar to PS-*b*-P4VP in DMF/THF, the specific details related to the initial micellar assembly and their packing following solvent evaporation are believed to be quite different.

The presence of the highly solvophobic PI end block introduces an additional enthalpic drive to minimize PI-solvent contact. Existing literature suggests that the resulting micelles likely contain a P4VP corona that encases a sphere composed of a PI core and a PS shell, a hypothesis supported by selectively stained TEM micrographs.[149] In contrast to the hexagonal packing of PS-*b*-P4VP, GISAXS studies suggest that cubic packings, particularly BCC, are preferred for PS-*b*-PI-*b*-P4VP in DOX/THF upon solvent evaporation.[154] After immersing these films in water, solvent/non-solvent exchange in the swollen P4VP coronae causes the chains to collapse along the significantly less swollen PS/PI cores. The collapse of the P4VP chains creates voids in the interstitial space between micelles, which are filled with non-solvent.[149] This process occurs in the top several layers of micelles at the film surface, converting the interstitial space between the micelles into an interconnected network of channels.[154,173] SEM images of the top surface of dried PS-*b*-PI-*b*-P4VP membranes demonstrate a square packing of surface pores with center-to-center distances that are consistent with the symmetry and lattice parameter of the initial cubic packing of micelles, suggesting that the evaporation-induced surface morphology is trapped upon precipitation.[149,154] The substructure retains a similar morphology to the previously discussed NIPS and PS-*b*-P4VP SNIPS membranes.

Film-Casting Strategies. The primary advantage of the SNIPS mechanism is that the resultant membranes contain integral selective and support layers. As a result, the desired architecture of a thin and highly size-selective active layer supported by a thicker and highly porous substructure is inherent to the process, eliminating the need for complex coating protocols involving porous substrates.[7,138,163] Instead, a concentrated solution of block polymer can be easily blade cast into a free-standing film using identical procedures to those commercially used in NIPS membranes. While these free-standing SNIPS membranes often exhibit similar water permeabilities and improved size-selectivities when compared to NIPS membranes with similar average pore sizes, they typically require large quantities of block polymer which can significantly raise the materials cost.[7] Furthermore, a large portion of the block polymer mass forms the highly porous substructure and does not significantly contribute to the overall size selectivity. The use of commercially produced block polymers (*e.g.*, PS-*b*-PB-*b*-PS) for SNIPS membranes could potentially reduce materials costs, but few reports have fully explored these polymers for membrane fabrication.[174] Therefore, processing methods that can reduce the thickness of this substructure without compromising the size selectivity and mechanical integrity are of high interest.

As discussed previously for selectively etched and selectively swollen systems, composite membranes are perhaps the most attractive solution. This can significantly reduce the thickness of the non-selective block polymer substructure without adversely affecting either the overall mechanical robustness or the high size selectivity. Thin selective layers of PS-*b*-P4VP have been spray coated onto PVDF or PAN membranes, reducing the total block polymer thickness from ~50 μm for a free-standing membrane to 1 μm for the composite membrane, without compromising solute rejection.[175] Additionally, roller casting methods that more closely resemble traditional membrane casting processes have been used to coat a thin PS-*b*-P4VP SNIPS layer on top of a PAN membrane.[176]

Due to the similarities between the pore formation mechanisms in SNIPS and NIPS, it is also possible to co-cast a NIPS-based solution and a SNIPS-based solution into a composite architecture.[177,178] This strategy follows a similar protocol as previously discussed for UF membranes derived from selectively etched disordered block polymers. Briefly, a homopolymer solution is first cast into a film followed by coating a block polymer solution on top of the nascent support layer. A partial evaporation step drives block polymer self-assembly at the surface of the active (top) layer, while the film remains highly swollen in solvent closer to the substrate. This film can then be immersed into a non-solvent bath to simultaneously induce pore formation in the homopolymer-derived support layer by NIPS and in the block polymer-derived selective layer by SNIPS. Such a strategy has been successfully reported for a PS-*b*-P4VP block polymer solution on top of a PS homopolymer solution.[177] However, adoption of this technique has been limited by the poor adhesion of the porous block polymer layer to porous sublayers formed from commercially relevant polymers, such as PAN.[177]

All of the coating methods discussed thus far have targeted flat sheet membrane configurations, but many industrially relevant separations processes use hollow fiber modules due to their higher packing efficiency and easier cleaning.[139] These hollow fiber configurations are usually obtained by extruding polymer solutions through a spinneret and into a coagulation bath. Due to its mechanistic similarities to NIPS, the SNIPS process should be readily integrated into the existing fiber spinning infrastructure.[157,177,178] There are numerous reports focused on the fabrication of hollow fiber SNIPS membranes, and they have been comprehensively discussed in a recent review.[139] In general, the overall mechanism is similar to the flat sheet configuration. A concentrated block polymer solution is extruded though an annular spinneret followed by a partial solvent evaporation step before the fiber enters the non-solvent bath. In addition to the key processing parameters discussed

https://dx.doi.org/10.1021/acsnano.0c07883
ACS Nano 2020, 14, 16446−16471

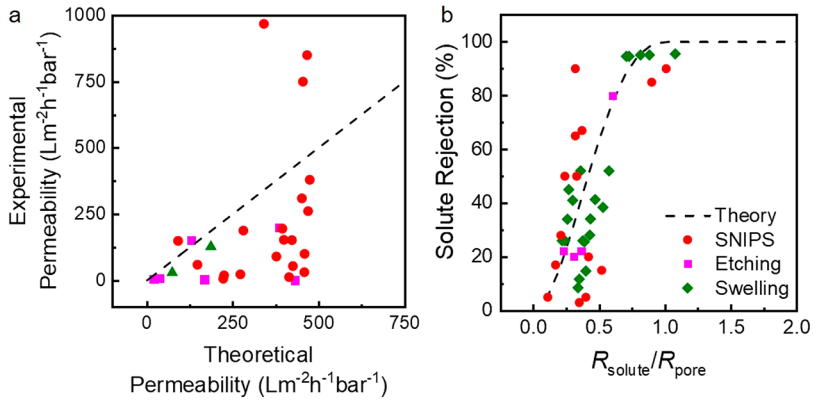

Figure 8. Scatter plot comparing the experimentally measured water permeability to the theoretical water permeability as estimated by the Hagen−Poiseuille equation for several block polymer membranes (a). The theoretical permeability was calculated according to a resistors-in-series model based on SEM images of the selective layer and the reported support layer permeability. The dashed line denotes the ideal case, where the experimental water permeability exactly matches the theoretical prediction. Three data points for SNIPS membranes have experimental permeabilities that are higher than their theoretical permeabilities, likely reflecting errors in the estimations of the support layer permeabilities for these systems. The experimental parameters and references corresponding to the presented data are provided in Table S1. BSA rejection ($R_h \approx 4$ nm) as a function of R_{solute}/R_{pore} is presented for several different block-polymer-derived UF membranes (b). The dashed line denotes the theoretical rejection curve for an isoporous membrane. The experimental parameters and references corresponding to the presented data are provided in Table S2.

previously, the morphology of fiber-spun SNIPS membranes depends upon the shear stresses in the spinneret, the block polymer flow rate, and the distance and time in air gap between the spinneret die and the non-solvent bath.[139] Either free-standing[137,179−182] or composite[175,177,178] hollow fiber SNIPS membranes can be fabricated. Hollow fiber composite membranes can be obtained by spray coating or dip coating a thin block polymer layer onto a porous substrate.[175] Additionally, co-casting techniques can be used to fabricate dual layer hollow fibers by passing both a block polymer solution and a homopolymer solution through a triple orifice spinneret followed by extrusion into a non-solvent bath, as has been demonstrated for PS-*b*-P4VP.[113]

Domain Alignment and Morphological Control. Regardless of the fabrication procedure, an appealing feature of the SNIPS process is that continuous pores are routinely obtained in the selective layer without having to orient the block polymer domains.[7,20,138] The evaporation of solvent from the film−air interface creates a driving force for self-assembly perpendicular to the film surface. Furthermore, the integral nature of the selective and support layers ensures that the pores in the selective layer are directly connected to the pores in the support layer with a gradient in pore sizes across the membrane thickness.[169] These features can significantly reduce membrane processing costs associated with the previously discussed magnetic field and SVA protocols, and these processing savings could potentially compensate for the increased materials cost of SNIPS membranes.

STRUCTURE−PROPERTY−PERFORMANCE RELATIONSHIPS IN BLOCK POLYMER UF MEMBRANES

While the lab-scale preparation of block polymer UF membranes is relatively mature and enhanced size selectivity over traditional UF membranes has been demonstrated, block polymer membranes must be economically competitive with existing NIPS membranes to be commercially viable. This requires water permeability comparable to NIPS membranes, tunable and sharp molecular weight cutoff values, high fouling resistance to minimize membrane cleaning and maximize operation lifetime, and rapid fabrication at a large scale and a low cost. To identify the core research areas, critical analysis of key structure−property−performance relationships must be performed. In this section, we will evaluate the water permeability, size selectivity, fouling resistance, and process scalability of state-of-the-art block polymer UF membranes to help guide future research.

Water Permeability. The water permeability of UF membranes is one of the most important considerations for commercial viability. Membranes with high water permeability require smaller membrane areas, shorter filtration times, and lower applied pressures, resulting in a small system footprint and high energy efficiency.[3] Based on the Hagen−Poiseuille model (eq 1), the water permeability for a free-standing block polymer membrane can be increased by decreasing the film thickness, increasing the pore size, and increasing the total porosity.[26] Generally, the pore size can be increased by increasing the block polymer molar mass.[21,120,153] However, large adjustments in the average pore size significantly alter the MWCO. Therefore, increasing the porosity could be a more robust approach that does not alter solute rejection. For selectively etched and selectively swollen membranes, this can be easily achieved by increasing the volume fraction of the pore-forming block, but very high porosities ($\varepsilon > 0.5$) are susceptible to pore collapse.[110]

Decreasing the thickness of the block polymer layer can also significantly increase the water permeability. Composite membranes with a thin block polymer layer on top of a thicker and more porous support can accomplish this objective without compromising the mechanical integrity, reducing the thickness of the block polymer from several micrometers to below 100 nm.[21,125,175] Modeling the water permeability for composite membranes is more challenging than for free-standing membranes, but a resistors-in-series approach is useful:[183,184]

$$P_{dual}^{-1} = P_{support}^{-1} + P_{selective}^{-1} + P_{interface}^{-1} \quad (2)$$

https://dx.doi.org/10.1021/acsnano.0c07883
ACS Nano 2020, 14, 16446−16471

This model inversely relates the resistance to water flow to the permeability (P) for each layer as well as to the interface between the layers.

Applying this model framework to composite membranes with selectively swollen or selectively etched block polymer selective layers is relatively straightforward. The water permeability of the block polymer selective layer can be calculated using the Hagen−Poiseuille equation (eq 1), while the water permeability of the support layer can be independently measured. The interfacial resistance, $P_{\text{interface}}^{-1}$, corresponds to discontinuities (*e.g.*, dead-end pores) at the selective-layer/support-layer interface, and was neglected in our calculations due to practical challenges in measuring or estimating this quantity experimentally.[157] The theoretical water permeability of these membranes calculated using eqs 1 and 2 can then be compared to the experimental water permeabilities that are widely reported in the literature (Figure 8a). Raw data used to calculate the experimental and theoretical water permeabilities are provided in Table S1 of the Supporting Information. Despite accounting for resistance from the support layer, the experimental water permeabilities are still significantly lower than the resistors-in-series model predicts, particularly for selectively etched membranes. These results suggest that the interface between the selective and support layers may have a substantial negative impact on the overall permeability.

Applying the resistors-in-series model to SNIPS membranes is more challenging due to the integral selective and support layers. This makes an independent measurement of the support layer water permeability impossible, but the water permeability of the selective layer can still be estimated based on the surface porosity, average pore size, and active layer thickness observed by SEM. The substructure permeability was conservatively estimated as 500 L m^{-2} h^{-1} bar^{-1} for the data presented in Figure 8a based on typical support layer permeabilities reported for other block polymer membranes. Plasma etching of the active layer could potentially reveal the underlying substructure, enabling more accurate measurements of the substructure permeability. However, such studies have not been reported to the best of our knowledge. The substructure morphology of SNIPS membranes is highly process dependent; therefore, our rough estimate of the support layer permeability likely contributes to the larger variability in the data as compared to the other block polymer membranes. In general, the experimental permeabilities were lower than predicted by the resistors-in-series model, with a few notable exceptions where the experimental permeability was higher than the model prediction. For those systems, the selected support layer permeability likely underestimated the true permeability.[149,154,185]

These lower-than-expected water permeabilities have hindered the development of block polymer membranes, as they are unable to match the performance of NIPS membranes. The inability of the resistors-in-series model to accurately predict the experimental water permeability regardless of the pore formation mechanism suggests that additional factors contribute significant resistance to water transport, particularly the layer interface which we neglected in our calculations. For composite membranes, the block polymer casting solvent could partially dissolve or swell the NIPS support, significantly reducing the support layer water permeability and porosity compared to measurements obtained prior to coating.[86,87]

Additionally, pore size is typically measured by SEM in the dry state, while membrane processes are performed in the wet state. The presence of water may partially swell the polymer chains lining the pores, effectively decreasing the pore size.[186,187] This phenomenon may be particularly pronounced for pores lined by polar and hydrophilic moieties (such as PEO, P2VP, and P4VP), which are prominent in selectively swollen and SNIPS membranes.[186] Equation 1 predicts a d^4 dependence of the water permeability on the pore diameter (porosity scales as d^2 for a fixed pore number density), so even minor differences in the measured pore size have a significant impact on the predicted water permeability. For example, a 10% smaller pore size would yield a 35% decrease in the theoretical water permeability.

Pore tortuosity could also have a significant impact on the experimental water permeability, increasing the effective path length for water transport and decreasing the permeability as compared to a perfectly straight pore. The experimental data more closely follow the theoretical prediction after accounting for a reasonable degree of pore tortuosity ($\tau \approx 1.5-3$), but the experimental permeabilities are still generally lower than expected. Additionally, the effective porosity of the block polymer selective layer could also be lower than inferred based on SEM of the membrane surface. As discussed earlier, water permeation requires pores that are continuous through the entire thickness of the selective layer, but many block polymer morphologies exhibit discontinuous grain boundaries that interrupt water transport and significantly reduce the water permeability. This is particularly evident in selectively etched cylindrical block polymers, where challenges in orienting the domains and achieving high water permeabilities are well-documented.[18,21,22] The selective swelling mechanism partially mitigates this challenge, as misaligned domains merge into continuous pores upon swelling.[19,125,129] This may explain the generally higher water permeabilities observed for selectively swollen membranes compared to selectively etched membranes, but this comes at the cost of increased tortuosity. The presence of discontinuous pores in the selective layer is less obvious for SNIPS membranes, but the possibility cannot be dismissed. Due to the kinetic nature of SNIPS, active layer pore growth may be arrested before these pores connect to those in the substructure, resulting in a dense interlayer that impedes water transport.[144,170]

To address these hypotheses, significant advances in membrane metrology are needed. Electron microtomography is expected to grow in importance as a powerful tool that enables the 3D reconstruction of the selective layer morphology at the nanoscale, facilitating quantitative analysis of pore continuity.[169,188] Focused ion beam SEM is particularly intriguing, as it is compatible with >100 nm thick films and can thus be used to reconstruct the entire selective layer morphology with high fidelity and a wide depth of field.[170,188] Additionally, developments in liquid cell electron microscopy can facilitate sample imaging in environments that better represent real membrane processes, which is critical for obtaining more accurate measurements of the pore size.[189] Nanoscale diffusion experiments, such as pulsed field gradient NMR, can directly monitor the tracer diffusion of isotopically labeled water through the membrane pores to investigate the presence of misaligned and discontinuous pores, estimate the pore tortuosity, and reveal nanoscale confinement effects.[190] Finally, simulations that accurately describe the non-equilibrium morphologies obtained after block polymer coating can

https://dx.doi.org/10.1021/acsnano.0c07883
ACS Nano 2020, 14, 16446−16471

illuminate nanostructure development.[191,192] Such advances can reveal the factors currently limiting the water permeability of block polymer membranes and guide the development of higher performing systems.

Size Selectivity. While high water permeability is necessary, the primary motivation for the development of block polymer membranes is their potential for highly size-selective separations.[3,7] Many emerging applications for UF require precise discrimination between contaminants of nearly identical sizes, which is currently impossible to achieve in a single pass for NIPS membranes.[3,8,44,45]

As discussed previously, UF membranes operate by a size-exclusion mechanism, where particles that are larger than the membrane pores are rejected. For a solute of hydrodynamic radius a, permeating a membrane pore of radius r_p, the size-dependent rejection profile can be accurately predicted by eq 3:[11]

$$R = 1 - \left[2\left(1 - \frac{a}{r_p}\right)^2 - \left(1 - \frac{a}{r_p}\right)^4\right] \exp\left[-0.7146\left(\frac{a}{r_p}\right)^2\right] \quad (3)$$

Equation 3 was derived from hindered transport theory and represents the convective flow of a spherical particle as it approaches a cylindrical capillary.[11,27] Complete rejection of a solute requires that all the membrane pores are smaller than the contaminant targeted for removal. Equation 3 assumes an isoporous size distribution, where all pores are identical with a radius of r_p. Such behavior is expected for block polymer UF membranes, but commercial NIPS membranes exhibit a broad distribution of pore sizes. For these systems, eq 3 can be integrated across the pore size distribution,[11] typically assuming a log-normal pore size distribution:

$$\bar{R} = \frac{\int_0^\infty R\mathrm{n}(r) r^4 \, \mathrm{d}r}{\int_0^\infty \mathrm{n}(r) r^4 \, \mathrm{d}r} \quad (4)$$

where R is the rejection for an isoporous membrane and $n(r)$ is the log-normal distribution of pore radii, defined as

$$n(r) = \frac{n_0}{r\sqrt{2\pi}} (\ln[1 + (\sigma/\bar{r})^2])^{-1/2} \times \exp\left\{\frac{-\left[\ln\left(\frac{r}{\bar{r}}\sqrt{1 + (\sigma/\bar{r})^2}\right)\right]^2}{2\ln[1 + (\sigma/\bar{r})^2]}\right\} \quad (5)$$

where $\bar{r}$ is the mean pore radius and σ is the pore radius standard deviation.[193] Using the isoporous model along with reported average pore sizes obtained in the dry state for select block polymer UF membranes, we compared the experimental rejections of bovine serum albumin (BSA) to the theoretical prediction of eq 3 (Figure 8b). The experimental BSA rejection data are provided in Table S2 of the Supporting Information. The experimental data closely follow theory, consistent with the expectation that block polymer selective layers are indeed composed of nearly uniform pore sizes.

These conclusions are corroborated by the significantly smaller pore size coefficient of variation (standard deviation divided by mean pore size, σ/μ) of block polymer UF membranes as compared to NIPS membranes based on measurements that we made from reported SEM images in the dry state (Figure 9a). Raw data used to calculate the coefficients of variation are provided in Table S3 of the Supporting Information. Interestingly, the pore size coefficient of variation of block polymer membranes also appears to depend upon the pore formation mechanism. SNIPS membranes tend to have a broader pore size coefficient of variation than selectively etched and selectively swollen membranes, although σ/μ is generally still narrower than for NIPS membranes. This may be related to the hybrid nature of the SNIPS mechanism, which combines aspects of both NIPS and block polymer self-assembly.[138,139] In contrast, selective swelling and selective etching of block polymer films are performed at thermodynamic equilibrium, where pores are formed from well-defined and uniform domains. Selectively etched disordered morphologies also exhibit comparatively narrow pore size distributions, as they have been kinetically

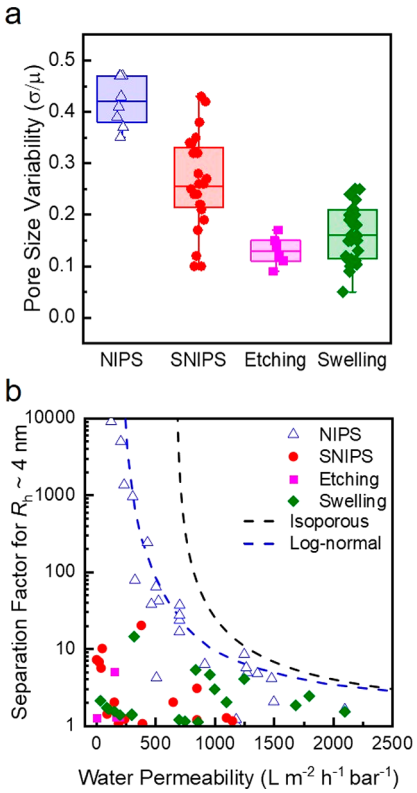

Figure 9. Pore size coefficient of variation (standard deviation, σ, divided by mean pore size, μ) is for traditional NIPS as well as block-polymer-derived UF membranes (a). The shaded boxes represent data that fall between the 25th and 75th percentiles, and the horizontal line in the center of the box represents the population median. The horizontal ticks outside the box represent the maximum and minimum of the population. The experimental parameters and references corresponding to the presented data are provided in Table S3. The separation factor, $(1 - \text{rejection})^{-1}$, for BSA ($R_h \approx 4$ nm) is presented against water permeability (b). All points correspond to experimentally reported values of permeability and rejection. Open blue triangles correspond to traditional NIPS membranes, while the filled symbols correspond to block polymer membranes. The solid line represents the theoretical separation factors calculated for isoporous pore size distributions, and the dashed line corresponds to a log-normal distribution, assuming a fixed ratio of surface porosity to active layer thickness (ε/δ) of 1 μm^{-1}.[11] The experimental parameters and references corresponding to the presented data are provided in Table S2.

https://dx.doi.org/10.1021/acsnano.0c07883
ACS Nano 2020, 14, 16446−16471

trapped in the equilibrium morphology associated with the processing temperature and conditions.[87,117] Overall, these high selectivities and nearly uniform pore sizes are encouraging, indicating that block polymer UF membranes satisfy their primary technological objective despite their lower than expected water permeabilities.

The ideal UF membrane would have both high water permeability and high size selectivity. However, examining the equations that describe the water permeability (eq 1) and the solute rejection (eq 3), small changes in the pore size can simultaneously have large effects on permeability and rejection for a constant ratio of surface porosity to active layer thickness (ε/δ). Practically, this reflects the well-discussed permeability−selectivity trade-off.[8,11] By simultaneously solving eq 1 and 3, it is possible to generate a permeability−selectivity curve for a given solute. Such a theoretical curve is presented in Figure 9b along with BSA rejection from both commercial NIPS and block polymer UF membranes. BSA was selected as a standard solute due to its ubiquity in the UF membrane literature. Experimental data are summarized in Table S2 in the Supporting Information.

Experimental data for NIPS membranes generally fall along a permeability−selectivity curve calculated assuming a log-normal pore size distribution and $\varepsilon/\delta = 1\ \mu m^{-1}$.[11] These assumptions reflect the broad pore size distributions and thin active layers of NIPS membranes.[3] Based on the reported range of porosities and selective layer thicknesses, block polymer membranes are expected to have ε/δ in the range of approximately 0.2 to 1 μm^{-1}. However, the experimental data generally fall well below this prediction. The sharp rejection curve shown in Figure 8b and the low pore size coefficient of variations shown in Figure 9a for block polymer membranes suggests that their comparatively poor performance does not reflect a low size selectivity. Instead, the lower selectivity likely results from a lower-than-expected water permeability. The low ratio of surface porosity to active layer thickness could reflect the well-documented challenges of coating very thin block polymer films and aligning the domains to generate continuous pores.[18] Additionally, as discussed in the previous section, the support layer has a significant effect on the overall permeability and may ultimately limit the permeability of composite membranes.

While BSA is an industry standard for evaluating UF membrane rejection, the R_h of BSA (~4 nm) is significantly smaller than the typical pore sizes of block polymer membranes, resulting in low separation factors. Virus filtration requires the rejection of solutes with $R_h \approx 10$ nm. Therefore, PEO with a molar mass of 100 kg mol^{-1} and $R_h \approx 10$ nm (PEO-100k) is a more representative standard to evaluate rejection for block polymer membranes (Figure 10). Experimental data is provided in Table S4 of the Supporting Information. In general, the separation factors were notably higher for PEO-100k than for BSA, indicating that block polymer membranes are more suitable for virus filtration than for the removal of small organic molecules, which is consistent with their typical pore sizes. However, the data still fall significantly below the predicted performance based on values of ε and δ obtained by SEM. For reference, a theoretical curve generated assuming $\varepsilon = 0.3$ and $\delta = 1\ \mu m$ (*i.e.*, typical values for block polymer UF membranes) is included in Figure 10. Again, this likely reflects significant contributions from the support layer to the overall permeability. Furthermore, support layer compaction may occur during operation. Highly

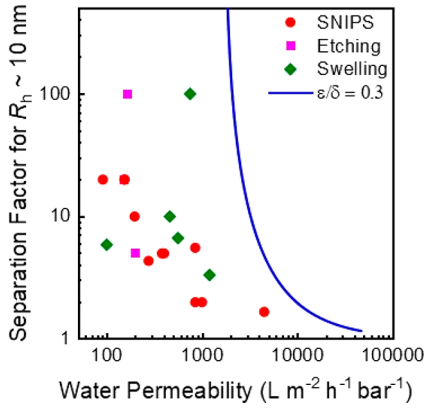

Figure 10. Separation factor, (1 − rejection)$^{-1}$, for PEO with a molar mass of 100 kg mol^{-1} and $R_h \approx 10$ nm that reasonably approximates the hydrodynamic size of viruses targeted in virus filtration. All points correspond to experimentally reported values of permeability and PEO-100k rejection. The isoporous theoretical curve was calculated assuming $\varepsilon = 0.3$ and $\delta = 1\ \mu m$, which are typical values for block polymer UF membranes. The experimental parameters and references corresponding to the presented data are provided in Table S4.

permeable NIPS membranes undergo compaction during operation, resulting in a decline in permeability over time due to a loss in porosity.[194,195] For composite block polymer membranes, this can result in water permeabilities that are significantly lower than expected. Additionally, most block polymer membranes have PS-based matrices with low toughness, which may exacerbate membrane compaction and flux decline. To advance block polymer membranes, their selectivities will need to become competitive with NIPS membranes. Fundamental studies investigating the role of the support layer in membrane performance are critical, with a particular focus on better understanding the morphological evolution during membrane operation. Future research should also focus on developing membrane matrix materials with improved toughness as well as fabrication methods for obtaining thinner selective layers with more continuous pores.

Fouling Resistance. Poor fouling resistance is a major limitation of commercial NIPS membranes due to their hydrophobic surfaces. Incorporating surface segregating amphiphilic block or comb polymers into the NIPS casting solution represents a straightforward strategy for easily improving the fouling resistance. These surface segregating block polymer additives can be readily integrated into the existing membrane casting infrastructure at low concentrations without requiring the often-complex coating procedures needed for block polymer selective layers. Consequently, these block polymer technologies are currently being incorporated into commercial membranes (see Ultramem produced by Clean Membranes), serving as a bridge between existing homopolymer NIPS membranes and next-generation block polymer membranes.[196]

The increased surface functionality of block polymers enables antifouling moieties to be chemically grafted to the membrane surface, improving their long-term stability over the physically bound additives employed in homopolymer NIPS membranes. Pyridine groups in P4VP-based SNIPS membranes are amenable to chemical functionalization, as demonstrated by the oxidation of a PS-*b*-P4VP membrane to form polyanionic PS-*b*-P4VPN-oxide.[197] Reactive handles can

https://dx.doi.org/10.1021/acsnano.0c07883
ACS Nano 2020, 14, 16446−16471

also be introduced along the pore walls of selectively etched membranes by incorporating a functional midblock or junction between the matrix-forming and sacrificial blocks. For example, the PI block of PS-*b*-PI-*b*-PLA was oxidized post-etching to produce reactive epoxide moieties along the pore walls.[198] Furthermore, selecting polymer segments with the desired functionality can eliminate the need for costly and often challenging functionalization steps. The SNIPS process is particularly attractive in this regard, as the pores are lined by a polar block (*e.g.*, P4VP, PAA, P2VP, PDMA). Inherently hydrophilic membranes have also been prepared through the selective swelling of block polymers, resulting in the enrichment of the polar block (*e.g.*, P2VP, PEO) along the membrane surface and pore walls.[129,136] Notably, a composite membrane prepared from an active layer of selectively swollen PS-*b*-PEO on a PVDF substrate displayed ∼100% recovery of the initial water flux after BSA filtration.[16] Blending amphiphilic block polymers into selectively etched membranes can also improve fouling resistance. This has been demonstrated for binary blends of PS-*b*-PEO and PS-*b*-PLA, where the miscibility between the PEO and PLA blocks resulted in a mixed PLA/PEO domain that was converted into PEO-lined pores upon PLA removal.[199] Overall, the potential for drastically improving the fouling resistance of UF membranes with block polymers represents a major advantage, potentially decreasing cleaning expenses and increasing membrane lifetime.

Process Scalability. Commercialization of block polymer UF membranes likely requires the continuous and roll-to-roll production of membranes at large size scales (>100 m^2) and low costs. Curtain coating represents the current industry standard for producing NIPS membranes. However, high-performing membranes fabricated from selectively etched or selectively swollen block polymers are typically obtained by difficult-to-scale processes, such as spin coating.[27,38] Furthermore, pore generation in these membranes often requires hours to days, in contrast to the instantaneous pore formation in NIPS. Recent advances have reduced the pore formation time to seconds by using microwave heating in conjunction with selective swelling, which is a promising development for more scalable fabrication.[135]

In this context, SNIPS membranes have risen to prominence, as they can be easily fabricated into highly permeable systems using blade coating techniques with near instantaneous pore formation. Due to the mechanistic similarities with NIPS, SNIPS membranes can be produced in a roll-to-roll process using existing industrial infrastructure, significantly increasing production throughput and reducing capital costs. Additionally, the SNIPS process can be easily integrated into fiber spinning processes, potentially enabling the production of more industrially relevant hollow fiber membrane modules, in contrast to the typical examples of flat-sheet block polymer UF membranes reported in the literature.[139,177,179,180] A major disadvantage of SNIPS membranes is their high materials cost, which is directly related to their integral and asymmetric architecture. Block polymer forms both the selective and support layers, yet only the thin selective layer contributes to the size selectivity. High materials costs may limit SNIPS membranes to high-value UF applications, but the ease and scalability of fabrication could potentially compensate for their high expenses. Additionally, composite SNIPS membranes can reduce the consumption of block polymer by up to 95%,[175,176] while co-casting strategies could potentially streamline production and lower costs even further.[177,178] Significant improvements in fouling resistance and toughness can also increase the operation lifetime of block polymer membranes compared to NIPS membranes, potentially mitigating their higher initial cost. Overall, the high cost of block polymer membranes may initially limit their usage to high-value applications (such as virus filtration, bioprocessing, and the process industry in general), where complete separation between solutes of similar sizes is crucial, rather than in wastewater treatment, where the multistep purification process can offset the relatively low size-selectivity of NIPS membranes. Commercial success in these high-value applications could lower fabrication costs and make block polymer membranes competitive in a broader array of applications.

FUTURE OUTLOOK

Achieving the technological objectives of block polymer membranes will require both fundamental research and practical advances in chemistry and processing. A number of open fundamental questions must be addressed to optimize membrane fabrication. Detailed studies of the non-equilibrium self-assembly and nanostructure formation during the SNIPS process can significantly guide membrane processing, reducing experimental time and costs and ensuring the reproducible fabrication of high-performing systems at an industrially relevant size scale. Understanding the contribution of the support layer to the overall performance of composite membranes is also necessary for optimizing membrane design. Furthermore, advances in characterization techniques are needed to provide robust and reliable data for more accurate predictions of the permeability and size selectivity of block polymer membranes. This will entail the continued development of microscopy techniques that facilitate imaging in 3D and in sample environments that better represent membrane operations.

The information gained from these fundamental studies is expected to significantly inform the synthetic design of block polymers specifically tailored for UF applications. The currently ubiquitous styrenic block polymers typically lack the necessary mechanical properties for commercial membrane processes. Polymer chemistries that replicate the performance of existing NIPS membranes are therefore required to achieve membranes that can withstand prolonged operation. These chemistries should be relatively cost-effective and transferable to industrial synthetic capabilities.

Furthermore, advances in membrane fabrication are critical. Many academic systems rely upon non-scalable coating process (*e.g.*, spin coating) or require large quantities of costly block polymer (*e.g.*, SNIPS membranes). Additionally, academic research has generally focused on the fabrication of flat sheet membranes; however, hollow fiber membranes are generally preferred by industry. Translation of lab-scale research to more commercially relevant membrane coating processes and configurations is crucial. Future developments must focus on reducing the cost or quantity of block polymer, reducing the time required for pore formation, and identifying coating methods that can be integrated into existing industrial membrane fabrication processes.

In summary, block polymer membranes represent a potentially transformative technology in water filtration. Superior size selectivities to existing NIPS membranes have been routinely demonstrated at the lab scale, introducing the possibility for more efficient and precise separations. This can

https://dx.doi.org/10.1021/acsnano.0c07883
ACS Nano 2020, 14, 16446−16471

improve process efficiency and foster the development of emerging applications. Furthermore, the enhanced functionality of block polymers allows for the incorporation of fouling resistant moieties that can significantly reduce cleaning expenses and extend membrane lifetimes. However, despite their immense potential, further progress is needed before block polymer membranes can supplant NIPS membranes. Identifying the optimal balance between maximizing water permeability and process scalability and minimizing materials costs is critical. The successful industrial adoption of block polymer UF membranes will require the identification of initial applications where the benefits associated with their high size selectivity, and potentially their high fouling resistance, outweigh their relatively higher materials costs. Block polymer membranes are slowly being commercialized at the start-up level,[200,201] and continued progress may transform these systems into commercially viable technologies.

ASSOCIATED CONTENT

Supporting Information

The Supporting Information is available free of charge at https://pubs.acs.org/doi/10.1021/acsnano.0c07883.

Detailed derivation of the Hagen−Poiseuille equation for polymer membranes. Tables S1−S4 compiling raw literature data on block polymer membrane pore sizes, water permeabilities, and rejection data used to construct Figure 8−10 (PDF)

AUTHOR INFORMATION

Corresponding Author

Marc A. Hillmyer − *Department of Chemistry, University of Minnesota, Minneapolis, Minnesota 55455, United States;* orcid.org/0000-0001-8255-3853; Email: hillmyer@umn.edu

Authors

Nicholas Hampu − *Department of Chemical Engineering and Materials Science, University of Minnesota, Minneapolis, Minnesota 55455, United States;* orcid.org/0000-0002-8127-1034

Jay R. Werber − *Department of Chemistry, University of Minnesota, Minneapolis, Minnesota 55455, United States*

Wui Yarn Chan − *Department of Chemistry, University of Minnesota, Minneapolis, Minnesota 55455, United States*

Elizabeth C. Feinberg − *Department of Chemistry, University of Minnesota, Minneapolis, Minnesota 55455, United States;* orcid.org/0000-0001-5551-3725

Complete contact information is available at: https://pubs.acs.org/10.1021/acsnano.0c07883

Notes

The authors declare no competing financial interest.

ACKNOWLEDGMENTS

The authors would thank to thank Dr. Caitlin Sample for carefully reviewing the manuscript. Funding for this work was provided by the National Science Foundation (DMR-1609459 and DMR- 2003454).

VOCABULARY

block polymer, polymer molecules comprising two or more chemically distinct polymer segments that are covalently linked into a single chain

self-assembly, the process of individual components organizing into a well-defined collective structure without external intervention due to specific and localized interactions

ultrafiltration, a separations process involving porous membranes intended to remove solutes that are approximately 1−100 nm in size

water permeability, the volumetric flux (volume flow per time per membrane area) of pure water normalized to the applied hydraulic pressure (pressure applied to the fluid, water in this case)

selectivity, the ability of membranes to discriminate between solutes of nearly identical size; a measure of the precision of the membrane's ability to reject solutes

isoporous membranes, membranes comprising pores with uniform size and shape that are ideal for achieving high selectivities

fouling, the adhesion of biological, organic, and inorganic matter to the surface and pore walls of a membrane, constricting the membrane pores and decreasing water permeability

REFERENCES

(1) Mekonnen, M. M.; Hoekstra, A. Y. Four Billion People Facing Severe Water Scarcity. *Sci. Adv.* **2016**, *2* (2), e1500323.

(2) Ercin, A. E.; Hoekstra, A. Y. Water Footprint Scenarios for 2050: A Global Analysis. *Environ. Int.* **2014**, *64*, 71−82.

(3) Werber, J. R.; Osuji, C. O.; Elimelech, M. Materials for next-Generation Desalination and Water Purification Membranes. *Nature Reviews Materials* **2016**, *1*, 16018.

(4) Park, H. B.; Kamcev, J.; Robeson, L. M.; Elimelech, M.; Freeman, B. D. Maximizing the Right Stuff: The Trade-Off between Membrane Permeability and Selectivity. *Science* **2017**, *356* (6343), eaab0530.

(5) Guillen, G. R.; Pan, Y.; Li, M.; Hoek, E. M. V. Preparation and Characterization of Membranes Formed by Nonsolvent Induced Phase Separation: A Review. *Ind. Eng. Chem. Res.* **2011**, *50* (7), 3798−3817.

(6) Nunes, S. P. Block Copolymer Membranes for Aqueous Solution Applications. *Macromolecules* **2016**, *49* (8), 2905−2916.

(7) Zhang, Y.; Sargent, J. L.; Boudouris, B. W.; Phillip, W. A. Nanoporous Membranes Generated from Self-Assembled Block Polymer Precursors: Quo Vadis? *J. Appl. Polym. Sci.* **2015**, *132* (21), 41683.

(8) Moon, J. D.; Freeman, B. D.; Hawker, C. J.; Segalman, R. A. Can Self-Assembly Address the Permeability/Selectivity Trade-Offs in Polymer Membranes? *Macromolecules* **2020**, *53* (14), 5649−5654.

(9) Sadeghi, I.; Kaner, P.; Asatekin, A. Controlling and Expanding the Selectivity of Filtration Membranes. *Chem. Mater.* **2018**, *30* (21), 7328−7354.

(10) van de Witte, P.; Dijkstra, P. J.; van den Berg, J. W. A.; Feijen, J. Phase Separation Processes in Polymer Solutions in Relation to Membrane Formation. *J. Membr. Sci.* **1996**, *117* (1), 1−31.

(11) Mehta, A.; Zydney, A. L. Permeability and Selectivity Analysis for Ultrafiltration Membranes. *J. Membr. Sci.* **2005**, *249* (1−2), 245−249.

(12) Mochizuki, S.; Zydney, A. L. Theoretical Analysis of Pore Size Distribution Effects on Membrane Transport. *J. Membr. Sci.* **1993**, *82* (3), 211−227.

(13) Bates, F. S.; Fredrickson, G. H. Block Copolymers - Designer Soft Materials. *Phys. Today* **1999**, *52* (2), 32−38.

(14) Bates, C. M.; Bates, F. S. 50th Anniversary Perspective: Block Polymers—Pure Potential. *Macromolecules* **2017**, *50* (1), 3−22.
(15) Jackson, E. A.; Hillmyer, M. A. Nanoporous Membranes Derived from Block Copolymers: From Drug Delivery to Water Filtration. *ACS Nano* **2010**, *4* (7), 3548−3553.
(16) Yang, H.; Wang, Z.; Lan, Q.; Wang, Y. Antifouling Ultrafiltration Membranes by Selective Swelling of Polystyrene/poly(ethylene Oxide) Block Copolymers. *J. Membr. Sci.* **2017**, *542*, 226−232.
(17) Shevate, R.; Kumar, M.; Karunakaran, M.; Hedhili, M. N.; Peinemann, K.-V. Polydopamine/Cysteine Surface Modified Isoporous Membranes with Self-Cleaning Properties. *J. Membr. Sci.* **2017**, *529*, 185−194.
(18) Phillip, W. A.; O'Neill, B.; Rodwogin, M.; Hillmyer, M. A.; Cussler, E. L. Self-Assembled Block Copolymer Thin Films as Water Filtration Membranes. *ACS Appl. Mater. Interfaces* **2010**, *2* (3), 847−853.
(19) Shi, X.; Wang, Z.; Wang, Y. Highly Permeable Nanoporous Block Copolymer Membranes by Machine-Casting on Nonwoven Supports: An Upscalable Route. *J. Membr. Sci.* **2017**, *533*, 201−209.
(20) Peinemann, K.-V.; Abetz, V.; Simon, P. F. W. Asymmetric Superstructure Formed in a Block Copolymer *via* Phase Separation. *Nat. Mater.* **2007**, *6*, 992.
(21) Querelle, S. E.; Jackson, E. A.; Cussler, E. L.; Hillmyer, M. A. Ultrafiltration Membranes with a Thin Poly(styrene)-B-Poly(isoprene) Selective Layer. *ACS Appl. Mater. Interfaces* **2013**, *5* (11), 5044−5050.
(22) Jackson, E. A.; Lee, Y.; Hillmyer, M. A. ABAC Tetrablock Terpolymers for Tough Nanoporous Filtration Membranes. *Macromolecules* **2013**, *46* (4), 1484−1491.
(23) Yang, S. Y.; Park, J.; Yoon, J.; Ree, M.; Jang, S. K.; Kim, J. K. Virus Filtration Membranes Prepared from Nanoporous Block Copolymers with Good Dimensional Stability under High Pressures and Excellent Solvent Resistance. *Adv. Funct. Mater.* **2008**, *18* (9), 1371−1377.
(24) Phillip, W. A.; Amendt, M.; O'Neill, B.; Chen, L.; Hillmyer, M. A.; Cussler, E. L. Diffusion and Flow Across Nanoporous Polydicyclopentadiene-Based Membranes. *ACS Appl. Mater. Interfaces* **2009**, *1* (2), 472−480.
(25) Epstein, N. On Tortuosity and the Tortuosity Factor in Flow and Diffusion through Porous Media. *Chem. Eng. Sci.* **1989**, *44* (3), 777−779.
(26) Phillip, W. A.; Rzayev, J.; Hillmyer, M. A.; Cussler, E. L. Gas and Water Liquid Transport through Nanoporous Block Copolymer Membranes. *J. Membr. Sci.* **2006**, *286* (1), 144−152.
(27) Baker, R. W. *Membrane Technology and Applications*, 3rd ed.; John Wiley & Sons: Chichester, West Sussex, UK, 2012.
(28) Wu, D.; Howell, J.; Field, R. Critical Flux Measurement for Model Colloids. *J. Membr. Sci.* **1999**, *152* (1), 89−98.
(29) Zhang, R.; Liu, Y.; He, M.; Su, Y.; Zhao, X.; Elimelech, M.; Jiang, Z. Antifouling Membranes for Sustainable Water Purification: Strategies and Mechanisms. *Chem. Soc. Rev.* **2016**, *45* (21), 5888−5924.
(30) Asatekin, A.; Kang, S.; Elimelech, M.; Mayes, A. M. Anti-Fouling Ultrafiltration Membranes Containing Polyacrylonitrile-Graft-Poly(ethylene Oxide) Comb Copolymer Additives. *J. Membr. Sci.* **2007**, *298* (1), 136−146.
(31) Maruf, S. H.; Wang, L.; Greenberg, A. R.; Pellegrino, J.; Ding, Y. Use of Nanoimprinted Surface Patterns to Mitigate Colloidal Deposition on Ultrafiltration Membranes. *J. Membr. Sci.* **2013**, *428*, 598−607.
(32) Cheryan, M. *Ultrafiltration and Microfiltration Handbook*, 2nd ed.; CRC Press: Boca Raton, FL, 1998.
(33) Zhang, Y.; Vallin, J. R.; Sahoo, J. K.; Gao, F.; Boudouris, B. W.; Webber, M. J.; Phillip, W. A. High-Affinity Detection and Capture of Heavy Metal Contaminants Using Block Polymer Composite Membranes. *ACS Cent. Sci.* **2018**, *4* (12), 1697−1707.
(34) Zhang, Z.; Rahman, M. M.; Abetz, C.; Höhme, A.-L.; Sperling, E.; Abetz, V. Chemically Tailored Multifunctional Asymmetric Isoporous Triblock Terpolymer Membranes for Selective Transport. *Adv. Mater.* **2020**, *32* (8), 1907014.
(35) Hoffman, J. R.; Phillip, W. A. 100th Anniversary of Macromolecular Science Viewpoint: Integrated Membrane Systems. *ACS Macro Lett.* **2020**, *9* (9), 1267−1279.
(36) Greenlee, L. F.; Lawler, D. F.; Freeman, B. D.; Marrot, B.; Moulin, P. Reverse Osmosis Desalination: Water Sources, Technology, and Today's Challenges. *Water Res.* **2009**, *43* (9), 2317−2348.
(37) Tchobanoglous, G.; Darby, J.; Bourgeous, K.; McArdle, J.; Genest, P.; Tylla, M. Ultrafiltration as an Advanced Tertiary Treatment Process for Municipal Wastewater. *Desalination* **1998**, *119* (1), 315−321.
(38) American Waterworks Association. *Microfiltration and Ultrafiltration Membranes for Drinking Water*, 2nd ed.; AWWA: Denver, CO, 2016.
(39) Jiang, Z.; Karan, S.; Livingston, A. G. Water Transport through Ultrathin Polyamide Nanofilms Used for Reverse Osmosis. *Adv. Mater.* **2018**, *30* (15), 1705973.
(40) Wen, C.; Huang, X.; Qian, Y. Domestic Wastewater Treatment Using an Anaerobic Bioreactor Coupled with Membrane Filtration. *Process Biochem.* **1999**, *35* (3), 335−340.
(41) Urgun-Demirtas, M.; Stark, B. C.; Pagilla, K. R. Comparison of 2-Chlorobenzoic Acid Biodegradation in a Membrane Bioreactor by *B. cepacia* and *B. cepacia* Bearing the Bacterial Hemoglobin Gene. *Water Res.* **2006**, *40* (16), 3123−3130.
(42) Salazar-Peláez, M. L.; Morgan-Sagastume, J. M.; Noyola, A. Influence of Hydraulic Retention Time on Fouling in a UASB Coupled with an External Ultrafiltration Membrane Treating Synthetic Municipal Wastewater. *Desalination* **2011**, *277* (1), 164−170.
(43) Cote, P.; Alam, Z.; Penny, J. Hollow Fiber Membrane Life in Membrane Bioreactors (MBR). *Desalination* **2012**, *288*, 145−151.
(44) Fallahianbijan, F.; Giglia, S.; Carbrello, C.; Bell, D.; Zydney, A. L. Impact of Protein Fouling on Nanoparticle Capture within the Viresolve® Pro and Viresolve® NFP Virus Removal Membranes. *Biotechnol. Bioeng.* **2019**, *116* (9), 2285−2291.
(45) van Reis, R.; Zydney, A. Bioprocess Membrane Technology. *J. Membr. Sci.* **2007**, *297* (1), 16−50.
(46) Wintgens, T.; Melin, T.; Schäfer, A.; Khan, S.; Muston, M.; Bixio, D.; Thoeye, C. The Role of Membrane Processes in Municipal Wastewater Reclamation and Reuse. *Desalination* **2005**, *178* (1), 1−11.
(47) Laîné, J.-M.; Vial, D.; Moulart, P. Status after 10 Years of Operation — Overview of UF Technology Today. *Desalination* **2000**, *131* (1), 17−25.
(48) Kimura, K.; Hane, Y.; Watanabe, Y.; Amy, G.; Ohkuma, N. Irreversible Membrane Fouling during Ultrafiltration of Surface Water. *Water Res.* **2004**, *38* (14), 3431−3441.
(49) Xiao, K.; Liang, S.; Wang, X.; Chen, C.; Huang, X. Current State and Challenges of Full-Scale Membrane Bioreactor Applications: A Critical Review. *Bioresour. Technol.* **2019**, *271*, 473−481.
(50) Lousada-Ferreira, M.; Geilvoet, S.; Moreau, A.; Atasoy, E.; Krzeminski, P.; van Nieuwenhuijzen, A.; van der Graaf. J. MLSS Concentration: Still a Poorly Understood Parameter in MBR Filterability. *Desalination* **2010**, *250* (2), 618−622.
(51) Drews, A.; Kraume, M. Process Improvement by Application of Membrane Bioreactors. *Chem. Eng. Res. Des.* **2005**, *83* (3), 276−284.
(52) Tiraferri, A.; Yip, N. Y.; Phillip, W. A.; Schiffman, J. D.; Elimelech, M. Relating Performance of Thin-Film Composite Forward Osmosis Membranes to Support Layer Formation and Structure. *J. Membr. Sci.* **2011**, *367* (1), 340−352.
(53) Vrijenhoek, E. M.; Hong, S.; Elimelech, M. Influence of Membrane Surface Properties on Initial Rate of Colloidal Fouling of Reverse Osmosis and Nanofiltration Membranes. *J. Membr. Sci.* **2001**, *188* (1), 115−128.
(54) Hester, J. F.; Olugebefola, S. C.; Mayes, A. M. Preparation of pH-Responsive Polymer Membranes by Self-Organization. *J. Membr. Sci.* **2002**, *208* (1), 375−388.

https://dx.doi.org/10.1021/acsnano.0c07883
ACS Nano 2020, 14, 16446−16471

(55) Hester, J. F.; Banerjee, P.; Mayes, A. M. Preparation of Protein-Resistant Surfaces on Poly(vinylidene Fluoride) Membranes *via* Surface Segregation. *Macromolecules* **1999**, *32* (5), 1643−1650.
(56) Hester, J. F.; Mayes, A. M. Design and Performance of Foul-Resistant Poly(vinylidene Fluoride) Membranes Prepared in a Single-Step by Surface Segregation. *J. Membr. Sci.* **2002**, *202* (1), 119−135.
(57) Asatekin, A.; Mayes, A. M. Antifouling Polymer Membranes with Subnanometer Size Selectivity. *Environ. Sci. Technol.* **2009**, *43* (12), 4487−4492.
(58) Kaner, P.; Dudchenko, A. V.; Mauter, M. S.; Asatekin, A. Zwitterionic Copolymer Additive Architecture Affects Membrane Performance: Fouling Resistance and Surface Rearrangement in Saline Solutions. *J. Mater. Chem. A* **2019**, *7* (9), 4829−4846.
(59) Zhao, W.; Su, Y.; Li, C.; Shi, Q.; Ning, X.; Jiang, Z. Fabrication of Antifouling Polyethersulfone Ultrafiltration Membranes Using Pluronic F127 as Both Surface Modifier and Pore-Forming Agent. *J. Membr. Sci.* **2008**, *318* (1), 405−412.
(60) Chen, W.; Su, Y.; Peng, J.; Zhao, X.; Jiang, Z.; Dong, Y.; Zhang, Y.; Liang, Y.; Liu, J. Efficient Wastewater Treatment by Membranes through Constructing Tunable Antifouling Membrane Surfaces. *Environ. Sci. Technol.* **2011**, *45* (15), 6545−6552.
(61) Zhao, X.; Su, Y.; Chen, W.; Peng, J.; Jiang, Z. pH-Responsive and Fouling-Release Properties of PES Ultrafiltration Membranes Modified by Multi-Functional Block-like Copolymers. *J. Membr. Sci.* **2011**, *382* (1), 222−230.
(62) Chen, W.; Su, Y.; Peng, J.; Dong, Y.; Zhao, X.; Jiang, Z. Engineering a Robust, Versatile Amphiphilic Membrane Surface Through Forced Surface Segregation for Ultralow Flux-Decline. *Adv. Funct. Mater.* **2011**, *21* (1), 191−198.
(63) Zhao, X.; Su, Y.; Li, Y.; Zhang, R.; Zhao, J.; Jiang, Z. Engineering Amphiphilic Membrane Surfaces Based on PEO and PDMS Segments for Improved Antifouling Performances. *J. Membr. Sci.* **2014**, *450*, 111−123.
(64) Bates, F. S.; Fredrickson, G. H. Block Copolymer Thermodynamics: Theory and Experiments. *Annu. Rev. Phys. Chem.* **1990**, *41*, 525−557.
(65) Rosedale, J. H.; Bates, F. S.; Almdal, K.; Mortensen, K.; Wignall, G. D. Order and Disorder in Symmetric Diblock Copolymer Melts. *Macromolecules* **1995**, *28* (5), 1429−1443.
(66) Sinturel, C.; Bates, F. S.; Hillmyer, M. A. High χ−Low N Block Polymers: How Far Can We Go? *ACS Macro Lett.* **2015**, *4* (9), 1044−1050.
(67) Yao, L.; Oquendo, L. E.; Schulze, M. W.; Lewis, R. M.; Gladfelter, W. L.; Hillmyer, M. A. Poly(cyclohexylethylene)-Block-Poly(lactide) Oligomers for Ultrasmall Nanopatterning Using Atomic Layer Deposition. *ACS Appl. Mater. Interfaces* **2016**, *8* (11), 7431−7439.
(68) Barreda, L.; Shen, Z.; Chen, Q. P.; Lodge, T. P.; Siepmann, J. I.; Hillmyer, M. A. Synthesis, Simulation, and Self-Assembly of a Model Amphiphile To Push the Limits of Block Polymer Nanopatterning. *Nano Lett.* **2019**, *19* (7), 4458−4462.
(69) Schmitt, A. K.; Mahanthappa, M. K. Characteristics of Lamellar Mesophases in Strongly Segregated Broad Dispersity ABA Triblock Copolymers. *Macromolecules* **2014**, *47* (13), 4346−4356.
(70) Widin, J. M.; Schmitt, A. K.; Im, K.; Schmitt, A. L.; Mahanthappa, M. K. Polydispersity-Induced Stabilization of a Disordered Bicontinuous Morphology in ABA Triblock Copolymers. *Macromolecules* **2010**, *43* (19), 7913−7915.
(71) Matsen, M. W.; Bates, F. S. Conformationally Asymmetric Block Copolymers. *J. Polym. Sci., Part B: Polym. Phys.* **1997**, *35* (6), 945−952.
(72) Bates, F. S.; Hillmyer, M. A.; Lodge, T. P.; Bates, C. M.; Delaney, K. T.; Fredrickson, G. H. Multiblock Polymers: Panacea or Pandora's Box? *Science* **2012**, *336* (6080), 434.
(73) Lequieu, J.; Koeper, T.; Delaney, K. T.; Fredrickson, G. H. Extreme Deflection of Phase Boundaries and Chain Bridging in A(BA′)n Miktoarm Star Polymers. *Macromolecules* **2020**, *53* (2), 513−522.
(74) Tang, P.; Qiu, F.; Zhang, H.; Yang, Y. Morphology and Phase Diagram of Complex Block Copolymers: ABC Star Triblock Copolymers. *J. Phys. Chem. B* **2004**, *108* (24), 8434−8438.
(75) Grason, G. M.; Kamien, R. D. Interfaces in Diblocks: A Study of Miktoarm Star Copolymers. *Macromolecules* **2004**, *37* (19), 7371−7380.
(76) Matsen, M. W. Fast and Accurate SCFT Calculations for Periodic Block-Copolymer Morphologies Using the Spectral Method with Anderson Mixing. *Eur. Phys. J. E: Soft Matter Biol. Phys.* **2009**, *30* (4), 361.
(77) Lodge, T. P. Block Copolymers: Long-Term Growth with Added Value. *Macromolecules* **2020**, *53* (1), 2−4.
(78) Li, L.; Szewczykowski, P.; Clausen, L. D.; Hansen, K. M.; Jonsson, G. E.; Ndoni, S. Ultrafiltration by Gyroid Nanoporous Polymer Membranes. *J. Membr. Sci.* **2011**, *384* (1), 126−135.
(79) Zhou, H.-J.; Yang, G.-W.; Zhang, Y.-Y.; Xu, Z.-K.; Wu, G.-P. Bioinspired Block Copolymer for Mineralized Nanoporous Membrane. *ACS Nano* **2018**, *12* (11), 11471−11480.
(80) Ting, Y.-H.; Park, S.-M.; Liu, C.-C.; Liu, X.; Himpsel, F. J.; Nealey, P. F.; Wendt, A. E. Plasma Etch Removal of Poly(methyl Methacrylate) in Block Copolymer Lithography. *Journal of Vacuum Science & Technology B: Microelectronics and Nanometer Structures Processing, Measurement, and Phenomena* **2008**, *26* (5), 1684−1689.
(81) Li, L.; Schulte, L.; Clausen, L. D.; Hansen, K. M.; Jonsson, G. E.; Ndoni, S. Gyroid Nanoporous Membranes with Tunable Permeability. *ACS Nano* **2011**, *5* (10), 7754−7766.
(82) Schulte, L.; Grydgaard, A.; Jakobsen, M. R.; Szewczykowski, P. P.; Guo, F.; Vigild, M. E.; Berg, R. H.; Ndoni, S. Nanoporous Materials from Stable and Metastable Structures of 1,2-PB-B-PDMS Block Copolymers. *Polymer* **2011**, *52* (2), 422−429.
(83) Vriezekolk, E. J.; Kudernac, T.; de Vos, W. M.; Nijmeijer, K. Composite Ultrafiltration Membranes with Tunable Properties Based on a Self-Assembling Block Copolymer/Homopolymer System. *J. Polym. Sci., Part B: Polym. Phys.* **2015**, *53* (21), 1546−1558.
(84) Lefèvre, N.; Daoulas, K. C.; Müller, M.; Gohy, J.-F.; Fustin, C.-A. Self-Assembly in Thin Films of Mixtures of Block Copolymers and Homopolymers Interacting by Hydrogen Bonds. *Macromolecules* **2010**, *43* (18), 7734−7743.
(85) Mao, H.; Hillmyer, M. A. Nanoporous Polystyrene by Chemical Etching of Poly(ethylene Oxide) from Ordered Block Copolymers. *Macromolecules* **2005**, *38* (9), 4038−4039.
(86) Vidil, T.; Hampu, N.; Hillmyer, M. A. Nanoporous Thermosets with Percolating Pores from Block Polymers Chemically Fixed above the Order−Disorder Transition. *ACS Cent. Sci.* **2017**, *3*, 1114.
(87) Hampu, N.; Hillmyer, M. A. Temporally Controlled Curing of Block Polymers in the Disordered State Using Thermally Stable Photoacid Generators for the Preparation of Nanoporous Membranes. *ACS Appl. Polym. Mater.* **2019**, *1* (5), 1148−1154.
(88) Cavicchi, K. A.; Zalusky, A. S.; Hillmyer, M. A.; Lodge, T. P. An Ordered Nanoporous Monolith from an Elastomeric Crosslinked Block Copolymer Precursor. *Macromol. Rapid Commun.* **2004**, *25* (6), 704−709.
(89) Chen, L.; Hillmyer, M. A. Mechanically and Thermally Robust Ordered Nanoporous Monoliths Using Norbornene-Functional Block Polymers. *Macromolecules* **2009**, *42* (12), 4237−4243.
(90) Phillip, W. A.; Hillmyer, M. A.; Cussler, E. L. Cylinder Orientation Mechanism in Block Copolymer Thin Films Upon Solvent Evaporation. *Macromolecules* **2010**, *43* (18), 7763−7770.
(91) Paradiso, S. P.; Delaney, K. T.; García-Cervera, C. J.; Ceniceros, H. D.; Fredrickson, G. H. Block Copolymer Self Assembly during Rapid Solvent Evaporation: Insights into Cylinder Growth and Stability. *ACS Macro Lett.* **2014**, *3* (1), 16−20.
(92) Hamley, I. W. Ordering in Thin Films of Block Copolymers: Fundamentals to Potential Applications. *Prog. Polym. Sci.* **2009**, *34* (11), 1161−1210.
(93) Fasolka, M. J.; Mayes, A. M. Block Copolymer Thin Films: Physics and Applications. *Annu. Rev. Mater. Res.* **2001**, *31*, 323−355.
(94) Segalman, R. A. Patterning with Block Copolymer Thin Films. *Mater. Sci. Eng., R* **2005**, *48* (6), 191−226.

https://dx.doi.org/10.1021/acsnano.0c07883
ACS Nano 2020, 14, 16446−16471

(95) Olayo-Valles, R.; Guo, S.; Lund, M. S.; Leighton, C.; Hillmyer, M. A. Perpendicular Domain Orientation in Thin Films of Polystyrene−Polylactide Diblock Copolymers. *Macromolecules* **2005**, *38* (24), 10101−10108.
(96) Han, E.; Stuen, K. O.; La, Y.-H.; Nealey, P. F.; Gopalan, P. Effect of Composition of Substrate-Modifying Random Copolymers on the Orientation of Symmetric and Asymmetric Diblock Copolymer Domains. *Macromolecules* **2008**, *41* (23), 9090−9097.
(97) Park, S.-M.; Stoykovich, M. P.; Ruiz, R.; Zhang, Y.; Black, C. T.; Nealey, P. F. Directed Assembly of Lamellae- Forming Block Copolymers by Using Chemically and Topographically Patterned Substrates. *Adv. Mater.* **2007**, *19* (4), 607−611.
(98) Sinturel, C.; Vayer, M.; Morris, M.; Hillmyer, M. A. Solvent Vapor Annealing of Block Polymer Thin Films. *Macromolecules* **2013**, *46* (14), 5399−5415.
(99) Baruth, A.; Seo, M.; Lin, C. H.; Walster, K.; Shankar, A.; Hillmyer, M. A.; Leighton, C. Optimization of Long-Range Order in Solvent Vapor Annealed Poly(styrene)-Block-Poly(lactide) Thin Films for Nanolithography. *ACS Appl. Mater. Interfaces* **2014**, *6* (16), 13770−13781.
(100) Feng, X.; Tousley, M. E.; Cowan, M. G.; Wiesenauer, B. R.; Nejati, S.; Choo, Y.; Noble, R. D.; Elimelech, M.; Gin, D. L.; Osuji, C. O. Scalable Fabrication of Polymer Membranes with Vertically Aligned 1 Nm Pores by Magnetic Field Directed Self-Assembly. *ACS Nano* **2014**, *8* (12), 11977−11986.
(101) Feng, X.; Kawabata, K.; Cowan, M. G.; Dwulet, G. E.; Toth, K.; Sixdenier, L.; Haji-Akbari, A.; Noble, R. D.; Elimelech, M.; Gin, D. L.; Osuji, C. O. Single Crystal Texture by Directed Molecular Self-Assembly along Dual Axes. *Nat. Mater.* **2019**, *18* (11), 1235−1243.
(102) Gopinadhan, M.; Deshmukh, P.; Choo, Y.; Majewski, P. W.; Bakajin, O.; Elimelech, M.; Kasi, R. M.; Osuji, C. O. Thermally Switchable Aligned Nanopores by Magnetic-Field Directed Self-Assembly of Block Copolymers. *Adv. Mater.* **2014**, *26* (30), 5148−5154.
(103) Majewski, P. W.; Gopinadhan, M.; Osuji, C. O. Magnetic Field Alignment of Block Copolymers and Polymer Nanocomposites: Scalable Microstructure Control in Functional Soft Materials. *J. Polym. Sci., Part B: Polym. Phys.* **2012**, *50* (1), 2−8.
(104) Choo, Y.; Mahajan, L. H.; Gopinadhan, M.; Ndaya, D.; Deshmukh, P.; Kasi, R. M.; Osuji, C. O. Phase Behavior of Polylactide-Based Liquid Crystalline Brushlike Block Copolymers. *Macromolecules* **2015**, *48* (22), 8315−8322.
(105) Cochran, E. W.; Garcia-Cervera, C. J.; Fredrickson, G. H. Stability of the Gyroid Phase in Diblock Copolymers at Strong Segregation. *Macromolecules* **2006**, *39* (7), 2449−2451.
(106) Matsen, M. W.; Bates, F. S. Origins of Complex Self-Assembly in Block Copolymers. *Macromolecules* **1996**, *29* (23), 7641−7644.
(107) Matsen, M. W.; Schick, M. Microphase Separation in Starblock Copolymer Melts. *Macromolecules* **1994**, *27* (23), 6761−6767.
(108) She, M.-S.; Lo, T.-Y.; Ho, R.-M. Controlled Ordering of Block Copolymer Gyroid Thin Films by Solvent Annealing. *Macromolecules* **2014**, *47* (1), 175−182.
(109) Jung, J.; Park, H.-W.; Lee, S.; Lee, H.; Chang, T.; Matsunaga, K.; Jinnai, H. Effect of Film Thickness on the Phase Behaviors of Diblock Copolymer Thin Film. *ACS Nano* **2010**, *4* (6), 3109−3116.
(110) Feng, X.; Imran, Q.; Zhang, Y.; Sixdenier, L.; Lu, X.; Kaufman, G.; Gabinet, U.; Kawabata, K.; Elimelech, M.; Osuji, C. O. Precise Nanofiltration in a Fouling-Resistant Self-Assembled Membrane with Water-Continuous Transport Pathways. *Sci. Adv.* **2019**, *5* (8), No. eaav9308.
(111) Seo, M.; Hillmyer, M. A. Reticulated Nanoporous Polymers by Controlled Polymerization-Induced Microphase Separation. *Science* **2012**, *336* (6087), 1422.
(112) Seo, M.; Moll, D.; Silvis, C.; Roy, A.; Querelle, S.; Hillmyer, M. A. Interfacial Polymerization of Reactive Block Polymers for the Preparation of Composite Ultrafiltration Membranes. *Ind. Eng. Chem. Res.* **2014**, *53* (48), 18575−18579.
(113) Hampu, N.; Bates, M. W.; Vidil, T.; Hillmyer, M. A. Bicontinuous Porous Nanomaterials from Block Polymers Radically Cured in the Disordered State for Size-Selective Membrane Applications. *ACS Appl. Nano Mater.* **2019**, *2*, 4567.
(114) Schulze, M. W.; Hillmyer, M. A. Tuning Mesoporosity in Cross-Linked Nanostructured Thermosets *via* Polymerization-Induced Microphase Separation. *Macromolecules* **2017**, *50* (3), 997−1007.
(115) Saba, S. A.; Mousavi, M. P. S.; Bühlmann, P.; Hillmyer, M. A. Hierarchically Porous Polymer Monoliths by Combining Controlled Macro- and Microphase Separation. *J. Am. Chem. Soc.* **2015**, *137* (28), 8896−8899.
(116) Oh, J.; Seo, M. Photoinitiated Polymerization-Induced Microphase Separation for the Preparation of Nanoporous Polymer Films. *ACS Macro Lett.* **2015**, *4* (11), 1244−1248.
(117) Hampu, N.; Hillmyer, M. A. Molecular Engineering of Nanostructures in Disordered Block Polymers. *ACS Macro Lett.* **2020**, *9* (3), 382−388.
(118) Yadav, M.; Bates, F. S.; Morse, D. C. Network Model of the Disordered Phase in Symmetric Diblock Copolymer Melts. *Phys. Rev. Lett.* **2018**, *121* (12), 127802.
(119) Hampu, N.; Werber, J. R.; Hillmyer, M. A. Co-Casting Highly Selective Dual Layer Membranes with Disordered Block Polymer Selective Layer. *ACS Appl. Mater. Interfaces* **2020**, *12* (40), 45351−45362.
(120) Wang, Y. Nondestructive Creation of Ordered Nanopores by Selective Swelling of Block Copolymers: Toward Homoporous Membranes. *Acc. Chem. Res.* **2016**, *49* (7), 1401−1408.
(121) Zhou, J.; Wang, Y. Selective Swelling of Block Copolymers: An Upscalable Greener Process to Ultrafiltration Membranes? *Macromolecules* **2020**, *53* (1), 5−17.
(122) Yin, J.; Yao, X.; Liou, J.-Y.; Sun, W.; Sun, Y.-S.; Wang, Y. Membranes with Highly Ordered Straight Nanopores by Selective Swelling of Fast Perpendicularly Aligned Block Copolymers. *ACS Nano* **2013**, *7* (11), 9961−9974.
(123) Shi, X.; Wang, X.; Wang, Y.; Wang, Y. Producing Nanoporosities in Block Copolymers within 30 S by Microwave-Boosted Selective Swelling. *Macromolecules* **2020**, *53*, 3619.
(124) Ahn, H.; Park, S.; Kim, S.-W.; Yoo, P. J.; Ryu, D. Y.; Russell, T. P. Nanoporous Block Copolymer Membranes for Ultrafiltration: A Simple Approach to Size Tunability. *ACS Nano* **2014**, *8* (11), 11745−11752.
(125) Yan, N.; Wang, Z.; Wang, Y. Highly Permeable Membranes Enabled by Film Formation of Block Copolymers on Water Surface. *J. Membr. Sci.* **2018**, *568*, 40−46.
(126) Guo, L.; Wang, Z.; Wang, Y. Perpendicular Alignment and Selective Swelling-Induced Generation of Homopores of Polystyrene-B-poly(2-Vinylpyridine)-B-Poly(ethylene Oxide) Triblock Terpolymer. *Macromolecules* **2018**, *51* (16), 6248−6256.
(127) Yang, H.; Guo, L.; Wang, Z.; Yan, N.; Wang, Y. Nanoporous Films with Superior Resistance to Protein Adsorption by Selective Swelling of Polystyrene-Block-Poly(ethylene Oxide). *Ind. Eng. Chem. Res.* **2016**, *55* (29), 8133−8140.
(128) Wang, Z.; Liu, R.; Yang, H.; Wang, Y. Nanoporous Polysulfones with *in Situ* PEGylated Surfaces by a Simple Swelling Strategy Using Paired Solvents. *Chem. Commun.* **2017**, *53* (65), 9105−9108.
(129) Zhong, D.; Wang, Z.; Lan, Q.; Wang, Y. Selective Swelling of Block Copolymer Ultrafiltration Membranes for Enhanced Water Permeability and Fouling Resistance. *J. Membr. Sci.* **2018**, *558*, 106−112.
(130) Wang, Y.; Zhang, C.; Zhou, J.; Wang, Y. Room-Temperature Swelling of Block Copolymers for Nanoporous Membranes with Well-Defined Porosities. *J. Membr. Sci.* **2020**, *608*, 118186.
(131) Christie, D.; Register, R. A.; Priestley, R. D. Direct Measurement of the Local Glass Transition in Self-Assembled Copolymers with Nanometer Resolution. *ACS Cent. Sci.* **2018**, *4* (4), 504−511.

https://dx.doi.org/10.1021/acsnano.0c07883
ACS Nano 2020, 14, 16446−16471

(132) Shi, X.; Xu, Z.; Huang, C.; Wang, Y.; Cui, Z. Selective Swelling of Electrospun Block Copolymers: From Perforated Nanofibers to High Flux and Responsive Ultrafiltration Membranes. *Macromolecules* **2018**, *51* (6), 2283−2292.
(133) Ma, D.; Zhou, J.; Wang, Z.; Wang, Y. Block Copolymer Ultrafiltration Membranes by Spray Coating Coupled with Selective Swelling. *J. Membr. Sci.* **2020**, *598*, 117656.
(134) Wang, Z.; Guo, L.; Wang, Y. Isoporous Membranes with Gradient Porosity by Selective Swelling of UV-Crosslinked Block Copolymers. *J. Membr. Sci.* **2015**, *476*, 449−456.
(135) Wang, Y.; Shi, X. S. *Method to Enhance the Process of Selective Swelling-Induced Pores Generation for Separation Membrane*. CN110124539A.
(136) Wang, Z.; Yao, X.; Wang, Y. Swelling-Induced Mesoporous Block Copolymer Membranes with Intrinsically Active Surfaces for Size-Selective Separation. *J. Mater. Chem.* **2012**, *22* (38), 20542−20548.
(137) Guo, L.; Wang, Y. Nanoslitting of Phase-Separated Block Copolymers by Solvent Swelling for Membranes with Ultrahigh Flux and Sharp Selectivity. *Chem. Commun.* **2014**, *50* (81), 12022−12025.
(138) Abetz, V. Isoporous Block Copolymer Membranes. *Macromol. Rapid Commun.* **2015**, *36* (1), 10−22.
(139) Radjabian, M.; Abetz, V. Advanced Porous Polymer Membranes from Self-Assembling Block Copolymers. *Prog. Polym. Sci.* **2020**, *102*, 101219.
(140) Weidman, J. L.; Mulvenna, R. A.; Boudouris, B. W.; Phillip, W. A. Nanostructured Membranes from Triblock Polymer Precursors as High Capacity Copper Adsorbents. *Langmuir* **2015**, *31* (40), 11113−11123.
(141) Zhang, Y.; Mulvenna, R. A.; Qu, S.; Boudouris, B. W.; Phillip, W. A. Block Polymer Membranes Functionalized with Nanoconfined Polyelectrolyte Brushes Achieve Sub-Nanometer Selectivity. *ACS Macro Lett.* **2017**, *6* (7), 726−732.
(142) Weidman, J. L.; Mulvenna, R. A.; Boudouris, B. W.; Phillip, W. A. Unusually Stable Hysteresis in the pH-Response of Poly(acrylic Acid) Brushes Confined within Nanoporous Block Polymer Thin Films. *J. Am. Chem. Soc.* **2016**, *138* (22), 7030−7039.
(143) Mulvenna, R. A.; Weidman, J. L.; Jing, B.; Pople, J. A.; Zhu, Y.; Boudouris, B. W.; Phillip, W. A. Tunable Nanoporous Membranes with Chemically-Tailored Pore Walls from Triblock Polymer Templates. *J. Membr. Sci.* **2014**, *470*, 246−256.
(144) Jung, A.; Rangou, S.; Abetz, C.; Filiz, V.; Abetz, V. Structure Formation of Integral Asymmetric Composite Membranes of Polystyrene-Block-Poly(2-Vinylpyridine) on a Nonwoven. *Macromol. Mater. Eng.* **2012**, *297* (8), 790−798.
(145) Schöttner, S.; Brodrecht, M.; Uhlein, E.; Dietz, C.; Breitzke, H.; Tietze, A. A.; Buntkowsky, G.; Gallei, M. Amine-Containing Block Copolymers for the Bottom-Up Preparation of Functional Porous Membranes. *Macromolecules* **2019**, *52* (7), 2631−2641.
(146) Schöttner, S.; Schaffrath, H.-J.; Gallei, M. Poly(2-Hydroxyethyl Methacrylate)-Based Amphiphilic Block Copolymers for High Water Flux Membranes and Ceramic Templates. *Macromolecules* **2016**, *49* (19), 7286−7295.
(147) Karunakaran, M.; Nunes, S. P.; Qiu, X.; Yu, H.; Peinemann, K.-V. Isoporous PS-B-PEO Ultrafiltration Membranes *via* Self-Assembly and Water-Induced Phase Separation. *J. Membr. Sci.* **2014**, *453*, 471−477.
(148) Hahn, J.; Filiz, V.; Rangou, S.; Clodt, J.; Jung, A.; Buhr, K.; Abetz, C.; Abetz, V. Structure Formation of Integral-Asymmetric Membranes of Polystyrene-Block-Poly(ethylene Oxide). *J. Polym. Sci., Part B: Polym. Phys.* **2013**, *51* (4), 281−290.
(149) Phillip, W. A.; Dorin, R. M.; Werner, J.; Hoek, E. M. V.; Wiesner, U.; Elimelech, M. Tuning Structure and Properties of Graded Triblock Terpolymer-Based Mesoporous and Hybrid Films. *Nano Lett.* **2011**, *11* (7), 2892−2900.
(150) Sutisna, B.; Polymeropoulos, G.; Musteata, V.; Peinemann, K.-V.; Avgeropoulos, A.; Smilgies, D.-M.; Hadjichristidis, N.; Nunes, S. P. Design of Block Copolymer Membranes Using Segregation Strength Trend Lines. *Mol. Syst. Des. Eng.* **2016**, *1* (3), 278−289.
(151) Clodt, J. I.; Filiz, V.; Rangou, S.; Buhr, K.; Abetz, C.; Höche, D.; Hahn, J.; Jung, A.; Abetz, V. Double Stimuli-Responsive Isoporous Membranes *via* Post-Modification of pH-Sensitive Self-Assembled Diblock Copolymer Membranes. *Adv. Funct. Mater.* **2013**, *23* (6), 731−738.
(152) Höhme, C.; Filiz, V.; Abetz, C.; Georgopanos, P.; Scharnagl, N.; Abetz, V. Postfunctionalization of Nanoporous Block Copolymer Membranes *via* Click Reaction on Polydopamine for Liquid Phase Separation. *ACS Appl. Nano Mater.* **2018**, *1* (7), 3124−3136.
(153) Shevate, R.; Kumar, M.; Cheng, H.; Hong, P.-Y.; Behzad, A. R.; Anjum, D.; Peinemann, K.-V. Rapid Size-Based Protein Discrimination inside Hybrid Isoporous Membranes. *ACS Appl. Mater. Interfaces* **2019**, *11* (8), 8507−8516.
(154) Gu, Y.; Wiesner, U. Tailoring Pore Size of Graded Mesoporous Block Copolymer Membranes: Moving from Ultrafiltration toward Nanofiltration. *Macromolecules* **2015**, *48* (17), 6153−6159.
(155) Zhang, Q.; Gu, Y.; Li, Y. M.; Beaucage, P. A.; Kao, T.; Wiesner, U. Dynamically Responsive Multifunctional Asymmetric Triblock Terpolymer Membranes with Intrinsic Binding Sites for Covalent Molecule Attachment. *Chem. Mater.* **2016**, *28* (11), 3870−3876.
(156) Zhu, G.; Ying, Y.; Li, X.; Liu, Y.; Yang, C.; Yi, Z.; Gao, C. Isoporous Membranes with Sub-10 Nm Pores Prepared from Supramolecular Interaction Facilitated Block Copolymer Assembly and Application for Protein Separation. *J. Membr. Sci.* **2018**, *566*, 25−34.
(157) Zhang, Y.; Mulvenna, R. A.; Boudouris, B. W.; Phillip, W. A. Nanomanufacturing of High-Performance Hollow Fiber Nanofiltration Membranes by Coating Uniform Block Polymer Films from Solution. *J. Mater. Chem. A* **2017**, *5* (7), 3358−3370.
(158) Rzayev, J.; Hillmyer, M. A. Nanochannel Array Plastics with Tailored Surface Chemistry. *J. Am. Chem. Soc.* **2005**, *127* (38), 13373−13379.
(159) Yu, H.; Qiu, X.; Moreno, N.; Ma, Z.; Calo, V. M.; Nunes, S. P.; Peinemann, K.-V. Self-Assembled Asymmetric Block Copolymer Membranes: Bridging the Gap from Ultra- to Nanofiltration. *Angew. Chem., Int. Ed.* **2015**, *54* (47), 13937−13941.
(160) Marques, D. S.; Vainio, U.; Chaparro, N. M.; Calo, V. M.; Bezahd, A. R.; Pitera, J. W.; Peinemann, K.-V.; Nunes, S. P. Self-Assembly in Casting Solutions of Block Copolymer Membranes. *Soft Matter* **2013**, *9* (23), 5557−5564.
(161) Capone, B.; Hansen, J.-P.; Coluzza, I. Competing Micellar and Cylindrical Phases in Semi-Dilute Diblock Copolymer Solutions. *Soft Matter* **2010**, *6* (24), 6075−6078.
(162) Oss-Ronen, L.; Schmidt, J.; Abetz, V.; Radulescu, A.; Cohen, Y.; Talmon, Y. Characterization of Block Copolymer Self-Assembly: From Solution to Nanoporous Membranes. *Macromolecules* **2012**, *45* (24), 9631−9642.
(163) Radjabian, M.; Abetz, C.; Fischer, B.; Meyer, A.; Abetz, V. Influence of Solvent on the Structure of an Amphiphilic Block Copolymer in Solution and in Formation of an Integral Asymmetric Membrane. *ACS Appl. Mater. Interfaces* **2017**, *9* (37), 31224−31234.
(164) Dreyer, O.; Wu, M.-L.; Radjabian, M.; Abetz, C.; Abetz, V. Structure of Nonsolvent-Quenched Block Copolymer Solutions after Exposure to Electric Fields during Solvent Evaporation. *Adv. Mater. Interfaces* **2019**, *6* (17), 1900646.
(165) Hahn, J.; Clodt, J. I.; Filiz, V.; Abetz, V. Protein Separation Performance of Self-Assembled Block Copolymer Membranes. *RSC Adv.* **2014**, *4* (20), 10252−10260.
(166) Dorin, R. M.; Marques, D. S.; Sai, H.; Vainio, U.; Phillip, W. A.; Peinemann, K.-V.; Nunes, S. P.; Wiesner, U. Solution Small-Angle X-Ray Scattering as a Screening and Predictive Tool in the Fabrication of Asymmetric Block Copolymer Membranes. *ACS Macro Lett.* **2012**, *1* (5), 614−617.
(167) Marques, D. S.; Dorin, R. M.; Wiesner, U.; Smilgies, D.-M.; Behzad, A. R.; Vainio, U.; Peinemann, K.-V.; Nunes, S. P. Time-Resolved GISAXS and Cryo-Microscopy Characterization of Block Copolymer Membrane Formation. *Polymer* **2014**, *55* (6), 1327−1332.

https://dx.doi.org/10.1021/acsnano.0c07883
ACS Nano 2020, 14, 16446−16471

(168) Stegelmeier, C.; Filiz, V.; Abetz, V.; Perlich, J.; Fery, A.; Ruckdeschel, P.; Rosenfeldt, S.; Förster, S. Topological Paths and Transient Morphologies during Formation of Mesoporous Block Copolymer Membranes. *Macromolecules* **2014**, *47* (16), 5566−5577.
(169) Sundaramoorthi, G.; Hadwiger, M.; Ben-Romdhane, M.; Behzad, A. R.; Madhavan, P.; Nunes, S. P. 3D Membrane Imaging and Porosity Visualization. *Ind. Eng. Chem. Res.* **2016**, *55* (12), 3689−3695.
(170) Nunes, S. P.; Sougrat, R.; Hooghan, B.; Anjum, D. H.; Behzad, A. R.; Zhao, L.; Pradeep, N.; Pinnau, I.; Vainio, U.; Peinemann, K.-V. Ultraporous Films with Uniform Nanochannels by Block Copolymer Micelles Assembly. *Macromolecules* **2010**, *43* (19), 8079−8085.
(171) Dorin, R. M.; Phillip, W. A.; Sai, H.; Werner, J.; Elimelech, M.; Wiesner, U. Designing Block Copolymer Architectures for Targeted Membrane Performance. *Polymer* **2014**, *55* (1), 347−353.
(172) Zhang, Q.; Li, Y. M.; Gu, Y.; Dorin, R. M.; Wiesner, U. Tuning Substructure and Properties of Supported Asymmetric Triblock Terpolymer Membranes. *Polymer* **2016**, *107*, 398−405.
(173) Pendergast, M. M.; Mika Dorin, R.; Phillip, W. A.; Wiesner, U.; Hoek, E. M. V. Understanding the Structure and Performance of Self-Assembled Triblock Terpolymer Membranes. *J. Membr. Sci.* **2013**, *444*, 461−468.
(174) Sutisna, B.; Polymeropoulos, G.; Musteata, V.; Sougrat, R.; Smilgies, D.-M.; Peinemann, K.-V.; Hadjichristidis, N.; Nunes, S. P. Functionalized Nanochannels from Self-Assembled and Photo-modified Poly(Styrene-B-Butadiene-B-Styrene). *Small* **2018**, *14* (18), 1701885.
(175) Hahn, J.; Clodt, J. I.; Abetz, C.; Filiz, V.; Abetz, V. Thin Isoporous Block Copolymer Membranes: It Is All about the Process. *ACS Appl. Mater. Interfaces* **2015**, *7* (38), 21130−21137.
(176) Bucher, T.; Filiz, V.; Abetz, C.; Abetz, V. Formation of Thin, Isoporous Block Copolymer Membranes by an Upscalable Profile Roller Coating Process—A Promising Way to Save Block Copolymer. *Membranes* **2018**, *8* (3), 57.
(177) Hilke, R.; Pradeep, N.; Behzad, A. R.; Nunes, S. P.; Peinemann, K.-V. Block Copolymer/Homopolymer Dual-Layer Hollow Fiber Membranes. *J. Membr. Sci.* **2014**, *472*, 39−44.
(178) Liu, Y.; Liu, T.; Su, Y.; Yuan, H.; Hayakawa, T.; Wang, X. Fabrication of a Novel PS4VP/PVDF Dual-Layer Hollow Fiber Ultrafiltration Membrane. *J. Membr. Sci.* **2016**, *506*, 1−10.
(179) Radjabian, M.; Koll, J.; Buhr, K.; Vainio, U.; Abetz, C.; Handge, U. A.; Abetz, V. Tailoring the Morphology of Self-Assembled Block Copolymer Hollow Fiber Membranes. *Polymer* **2014**, *55* (13), 2986−2997.
(180) Radjabian, M.; Koll, J.; Buhr, K.; Handge, U. A.; Abetz, V. Hollow Fiber Spinning of Block Copolymers: Influence of Spinning Conditions on Morphological Properties. *Polymer* **2013**, *54* (7), 1803−1812.
(181) Hilke, R.; Pradeep, N.; Madhavan, P.; Vainio, U.; Behzad, A. R.; Sougrat, R.; Nunes, S. P.; Peinemann, K.-V. Block Copolymer Hollow Fiber Membranes with Catalytic Activity and pH-Response. *ACS Appl. Mater. Interfaces* **2013**, *5* (15), 7001−7006.
(182) Sankhala, K.; Koll, J.; Radjabian, M.; Handge, U. A.; Abetz, V. A Pathway to Fabricate Hollow Fiber Membranes with Isoporous Inner Surface. *Adv. Mater. Interfaces* **2017**, *4* (7), 1600991.
(183) Werber, J. R.; Porter, C. J.; Elimelech, M. A Path to Ultraselectivity: Support Layer Properties To Maximize Performance of Biomimetic Desalination Membranes. *Environ. Sci. Technol.* **2018**, *52* (18), 10737−10747.
(184) Henis, J. M. S.; Tripodi, M. K. Composite Hollow Fiber Membranes for Gas Separation: The Resistance Model Approach. *J. Membr. Sci.* **1981**, *8* (3), 233−246.
(185) Gu, Y.; Dorin, R. M.; Wiesner, U. Asymmetric Organic−Inorganic Hybrid Membrane Formation *via* Block Copolymer−Nanoparticle Co-Assembly. *Nano Lett.* **2013**, *13* (11), 5323−5328.
(186) Rangou, S.; Buhr, K.; Filiz, V.; Clodt, J. I.; Lademann, B.; Hahn, J.; Jung, A.; Abetz, V. Self-Organized Isoporous Membranes with Tailored Pore Sizes. *J. Membr. Sci.* **2014**, *451*, 266−275.
(187) Wang, J.; Rahman, M. M.; Abetz, C.; Abetz, V. Bovine Serum Albumin Selective Integral Asymmetric Isoporous Membrane. *J. Membr. Sci.* **2020**, *604*, 118074.
(188) Feng, X.; Burke, C. J.; Zhuo, M.; Guo, H.; Yang, K.; Reddy, A.; Prasad, I.; Ho, R.-M.; Avgeropoulos, A.; Grason, G. M.; Thomas, E. L. Seeing Mesoatomic Distortions in Soft-Matter Crystals of a Double-Gyroid Block Copolymer. *Nature* **2019**, *575* (7781), 175−179.
(189) Parent, L. R.; Bakalis, E.; Proetto, M.; Li, Y.; Park, C.; Zerbetto, F.; Gianneschi, N. C. Tackling the Challenges of Dynamic Experiments Using Liquid-Cell Transmission Electron Microscopy. *Acc. Chem. Res.* **2018**, *51* (1), 3−11.
(190) Timachova, K.; Sethi, G. K.; Bhattacharya, R.; Villaluenga, I.; Balsara, N. P. Ion Diffusion across a Disorder-to-Order Phase Transition in a Poly(ethylene Oxide)-B-Poly(silsesquioxane) Block Copolymer Electrolyte. *Mol. Syst. Des. Eng.* **2019**, *4* (2), 357−364.
(191) Howard, M. P.; Lequieu, J.; Delaney, K. T.; Ganesan, V.; Fredrickson, G. H.; Truskett, T. M. Connecting Solute Diffusion to Morphology in Triblock Copolymer Membranes. *Macromolecules* **2020**, *53*, 2336.
(192) Wang, C.; Quan, X.; Liao, M.; Li, L.; Zhou, J. Computer Simulations on the Channel Membrane Formation by Nonsolvent Induced Phase Separation. *Macromol. Theory Simul.* **2017**, *26* (5), 1700027.
(193) Belfort, G.; Pimbley, J. M.; Greiner, A.; Chung, K. Y. Diagnosis of Membrane Fouling Using a Rotating Annular Filter. 1. Cell Culture Media. *J. Membr. Sci.* **1993**, *77* (1), 1−22.
(194) Bohonak, D. M.; Zydney, A. L. Compaction and Permeability Effects with Virus Filtration Membranes. *J. Membr. Sci.* **2005**, *254* (1), 71−79.
(195) Persson, K. M.; Gekas, V.; Trägårdh, G. Study of Membrane Compaction and Its Influence on Ultrafiltration Water Permeability. *J. Membr. Sci.* **1995**, *100* (2), 155−162.
(196) Lorain, O.; Espenan, J.-M.; Remigy, J.-F.; Rouch, J.-C.; Savart, T.; Gerard, P.; Magnet, S. *Copolymer Having Amphiphilic Blocks, and Use Thereof for Manufacturing Polymer Filtration Membranes*. US20160030896A1.
(197) Shevate, R.; Karunakaran, M.; Kumar, M.; Peinemann, K.-V. Polyanionic pH-Responsive Polystyrene-B-poly(4-Vinyl Pyridine-N-Oxide) Isoporous Membranes. *J. Membr. Sci.* **2016**, *501*, 161−168.
(198) Bailey, T. S.; Rzayev, J.; Hillmyer, M. A. Routes to Alkene and Epoxide Functionalized Nanoporous Materials from Poly(styrene-B-Isoprene-B-Lactide) Triblock Copolymers. *Macromolecules* **2006**, *39* (25), 8772−8781.
(199) Mao, H.; Hillmyer, M. A. Morphological Behavior of Polystyrene-Block-Polylactide/Polystyrene-Block-Poly(ethylene Oxide) Blends. *Macromol. Chem. Phys.* **2008**, *209* (16), 1647−1656.
(200) *Anfiro Inc. Technology Page*. http://www.anfiro.com/tech (accessed November 17, 2020).
(201) *Terapore Technologies Home Page*. https://www.terapore.com (accessed November 17, 2020).

https://dx.doi.org/10.1021/acsnano.0c07883
ACS Nano 2020, 14, 16446−16471